# MutSβ Stimulates Holliday Junction Resolution by the SMX Complex

## Graphical Abstract



## Highlights

- MutSβ, but not MutSα, interacts directly with SLX4

- MutSβ stimulates the resolution of recombination intermediates by SMX

- Defects in MutSβ lead to the accumulation of unresolved anaphase bridges at mitosis

- MutSβ is required for efficient Holliday junction resolution and genome stability
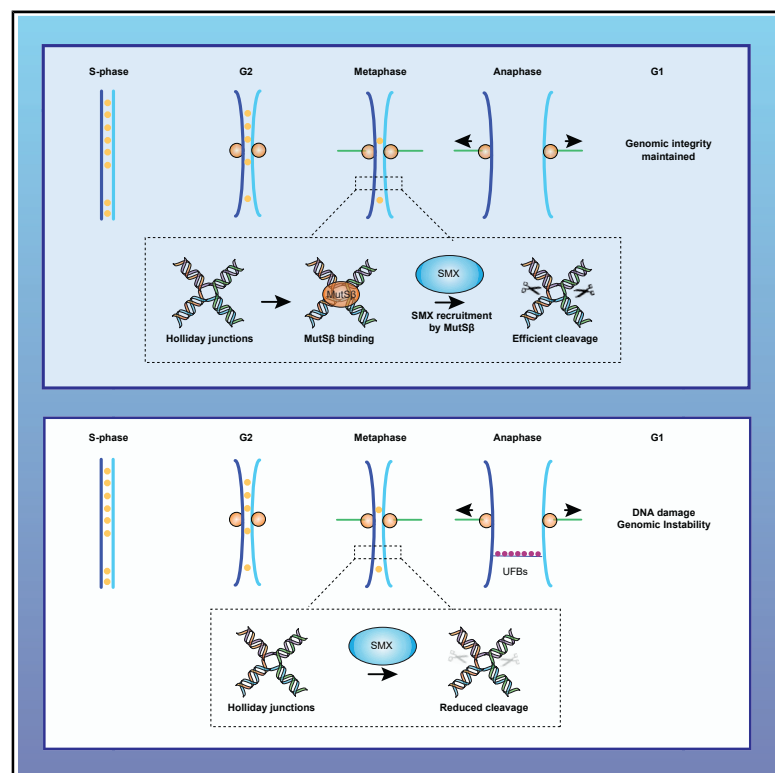
## Authors

Sarah J. Young, Marie Sebald, Rajvee Shah Punatar, ..., Monica C. Rodrigo-Brenni, Chih-Chao Liang, Stephen C. West

## Correspondence

stephen.west@crick.ac.uk

## In Brief

Young et al. show that MSH2 and MSH3, two components of the MutSβ heterodimer, bind SLX4 and are required for the efficient resolution of Holliday junctions by the SMX trinuclease complex. Loss of MutSβ activity leads to an accumulation of unresolved homologous recombination ultrafine bridges at mitosis.

## Article

# MutSβ Stimulates Holliday Junction Resolution by the SMX Complex

Sarah J. Young,[1] Marie Sebald,[1] Rajvee Shah Punatar,[1] Meghan Larin,[1,2] Laura Masino,[1] Monica C. Rodrigo-Brenni,[1,3] Chih-Chao Liang,[1] and Stephen C. West[1,4,*]

[1]The Francis Crick Institute, 1 Midland Road, London NW1 1AT, UK
[2]Present address: Dementia Research Institute, Cardiff University, Maindy Road, Cardiff CF24 4HQ, UK
[3]Present address: AstraZeneca, 1 Francis Crick Avenue, Trumpington, Cambridge CB2 0AA, UK
[4]Lead Contact
*Correspondence: stephen.west@crick.ac.uk
https://doi.org/10.1016/j.celrep.2020.108289

## SUMMARY

MutSα and MutSβ play important roles in DNA mismatch repair and are linked to inheritable cancers and degenerative disorders. Here, we show that MSH2 and MSH3, the two components of MutSβ, bind SLX4 protein, a scaffold for the assembly of the SLX1-SLX4-MUS81-EME1-XPF-ERCC1 (SMX) trinuclease complex. SMX promotes the resolution of Holliday junctions (HJs), which are intermediates in homologous recombinational repair. We find that MutSβ binds HJs and stimulates their resolution by SLX1-SLX4 or SMX in reactions dependent upon direct interactions between MutSβ and SLX4. In contrast, MutSα does not stimulate HJ resolution. MSH3-depleted cells exhibit reduced sister chromatid exchanges and elevated levels of homologous recombination ultrafine bridges (HR-UFBs) at mitosis, consistent with defects in the processing of recombination intermediates. These results demonstrate a role for MutSβ in addition to its established role in the pathogenic expansion of CAG/CTG trinucleotide repeats, which is causative of myotonic dystrophy and Huntington's disease.

## INTRODUCTION

The accurate processing of branched DNA intermediates that form during replication, recombination, and repair is essential for the maintenance of genomic integrity and the prevention of cancer (Dehé and Gaillard, 2017). During the repair of double-strand breaks (DSBs) by homologous recombination (HR), covalent four-way DNA linkages known as Holliday junctions (HJs) form between sister chromatids. If these structures are not efficiently processed, cells display high levels of DNA damage and chromosomal instability (Chan et al., 2018; Sarbajna et al., 2014; Wechsler et al., 2011).

Human cells process HJs by two mechanisms: (1) dissolution by the BLM-TopoIIIα-RMI1-RMI2 (BTR) complex (Singh et al., 2008; Wu et al., 2006; Wu and Hickson, 2003) or (2) nucleolytic resolution by the SLX1-SLX4-MUS81-EME1-XPF-ERCC1 (SMX) complex or GEN1 (Castor et al., 2013; Garner et al., 2013; Ip et al., 2008; Muñoz et al., 2009; Svendsen et al., 2009; Wechsler et al., 2011; Wyatt et al., 2017). Dissolution defects are observed in Bloom's syndrome cells, mutated for *BLM*, and are associated with a high frequency of sister chromatid exchanges (SCEs) and cancer predisposition (Chaganti et al., 1974; German, 1993). Increased SCE formation can be suppressed by loss of GEN1 or components of SMX, indicating that they arise from unscheduled resolution events (Wechsler et al., 2011). Cells carrying mutations in SLX4/MUS81 and GEN1 display a high incidence of lagging chromosomes and ul-

trafine DNA bridge formation during mitotic anaphase, resulting in DNA breakage and cell death (Chan et al., 2018; Garner et al., 2013; Sarbajna et al., 2014; Wechsler et al., 2011).

SLX4 protein (200 kDa) acts as a multidomain scaffold for assembly of the structure-selective endonucleases (SSEs) that comprise the SMX complex by making direct interactions with SLX1, MUS81, and XPF (Fekairi et al., 2009; Muñoz et al., 2009; Svendsen et al., 2009). SLX1 and SLX4 form an obligate heterodimer, and SLX4 constitutively interacts with a subset of the XPF-ERCC1 present in the cell (Wyatt et al., 2017). In contrast, the interaction of MUS81-EME1 with SLX4 requires CDK1 and PLK1-mediated phosphorylation and is restricted to the late stages of the cell cycle (Duda et al., 2016; Wyatt et al., 2013). This interaction allows the N-terminal domain of MUS81 to adopt an open conformation, activating MUS81-EME1 by relaxation of its substrate specificity. As such, the activated SMX complex forms a highly promiscuous trinuclease that can cleave HJs, 5′- and 3′-flaps, and replication forks (Wyatt et al., 2017). Limiting the actions of SMX to mitosis prevents cleavage of replication forks during S phase, whereas replication/recombination intermediates that persist until G2/M are efficiently cleaved prior to the separation of sister chromatids. GEN1, which is primarily cytoplasmic, provides a backup pathway of cleavage that comes into play upon breakdown of the nuclear envelope (Chan and West, 2014).

The SLX4-associated SSEs (SLX1, MUS81-EME1, and XPF-ERCC1) play key roles in multiple aspects of DNA metabolism,
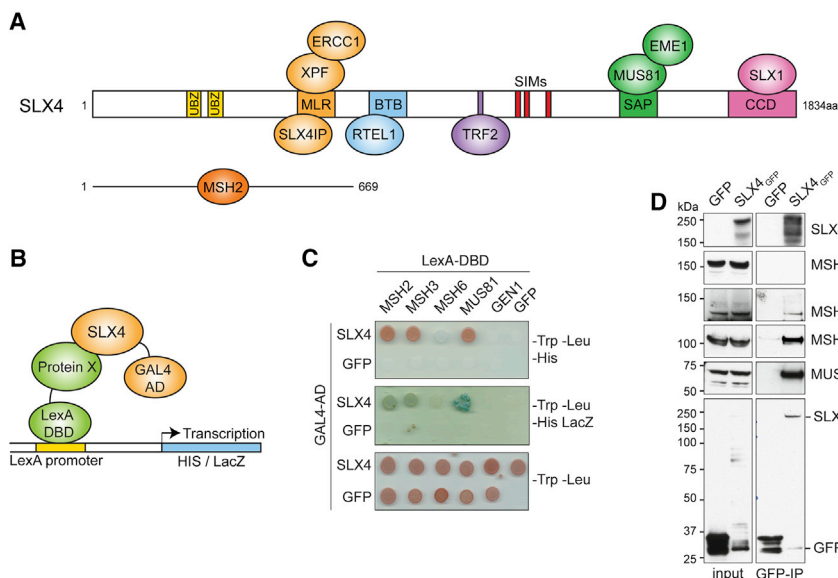
**Figure 1. Interactions between SLX4 and MutSβ**

(A) Schematic diagram of human SLX4 protein. Selected functional domains and interaction partners are indicated. MSH2 interacts with a region encompassing the first 669 aa of SLX4. UBZ, ubiquitin-binding zinc-finger domain; MLR, MUS312/MEI-9 interaction like region; BTB, broad complex-tram-track-bric-a-brac domain; SIMs, SUMO-interacting motifs; SAP, SAF-A/B-Acinus and PAIS domain; CCD, coiled-coil domain.

(B) Schematic of the yeast-two-hybrid assay. Proteins of interest were fused to the activation domain (AD) of GAL4 or the DNA binding domain (DBD) of LexA as indicated.

(C) Interactions between SLX4 and the indicated proteins using yeast-two-hybrid analysis.

(D) HEK293T cells were transiently transfected with plasmids expressing GFP or SLX4$_{GFP}$, and GFP was immunoprecipitated from cell-free extracts. SLX4$_{GFP}$-interacting proteins were detected using antibodies against SLX4, MSH2, MSH3, MSH6, MUS81, or GFP.

including replication fork stability, common fragile site (CFS) expression, telomere length maintenance, and the repair of DNA inter-strand crosslinks (ICLs) (Guervilly and Gaillard, 2018). Cells lacking SLX4 are sensitive to a range of agents that induce ICL damage, DNA alkylation, or replication stress (Crossan and Patel, 2012; Kim et al., 2013; Muñoz et al., 2009; Svendsen et al., 2009), and *SLX4*$^{-/-}$ mice are born at sub-Mendelian ratios and are cancer prone (Castor et al., 2013; Crossan et al., 2011; Hodskinson et al., 2014; Holloway et al., 2011). In humans, biallelic mutations in *SLX4* or *XPF* cause Fanconi anemia (subgroups *FANCP* and *FANCQ*, respectively), an inheritable disease characterized by developmental abnormalities, an inability to repair ICLs, and cancer susceptibility (Bogliolo et al., 2013; Kim et al., 2011; Stoepker et al., 2011). These observations highlight the importance of SLX4, and associated complexes, for genomic stability.

In addition to its interaction with the three nucleases, SLX4 also interacts with proteins involved in mismatch repair (MMR; MSH2, MSH3, and MSH6) and telomere maintenance (TRF2, RTEL1, and SLX4IP), as determined by mass spectrometry (González-Prieto et al., 2015; Svendsen et al., 2009; Takedachi et al., 2020; Wu et al., 2020; Zhang et al., 2019). The MSH proteins form two heterodimeric ATPases, MutSα (MSH2-MSH6) and MutSβ (MSH2-MSH3), which are key components of the MMR system that removes errors incorporated during DNA replication (Fishel, 2015). Defects in MMR cause the autosomal genetic disorder Lynch syndrome (hereditary non-polyposis colorectal cancer), a disease characterized by high mutation rates, microsatellite instability, and cancer predisposition (Duraturo et al., 2019; Fishel et al., 1993).

MutSα and MutSβ play distinct roles in MMR; MutSα binds to single-nucleotide mismatches and 1- to 2-nt insertions (Alani, 1996; Drummond et al., 1995; Gradia et al., 1997; Iaccarino et al., 1996; Marsischky et al., 1996), whereas MutSβ binds small heteroduplex loops (Acharya et al., 1996; Genschel et al., 1998; Wilson et al., 1999). Mismatch recognition induces the ATP-

dependent activation of MutLα endonuclease, which cleaves the DNA to initiate lesion removal (Constantin et al., 2005; Kadyrov et al., 2006; Pluciennik et al., 2010). In contrast to MutSα, the DNA binding pocket of MutSβ can accommodate DNA with a range of different bending angles (Constantin et al., 2005; Genschel et al., 1998; Gupta et al., 2011; Wilson et al., 1999). It can therefore bind a variety of branched DNA structures *in vitro* and plays a broader role in DNA metabolism (Surtees and Alani, 2006). For example, MutSβ promotes the pathogenic expansion of CAG/CTG trinucleotide repeats, which are causative of more than a dozen degenerative disorders, including myotonic dystrophy and Huntington's disease (Iyer et al., 2015). Trinucleotide repeats form large heteroduplex loops/hairpins that are bound by MutSβ. However, these structures are refractory to repair, and binding by MutSβ leads to their pathogenic instability (Hou et al., 2009; Keogh et al., 2017; Panigrahi et al., 2010; Tian et al., 2009).

Interestingly, like SLX4 complexes, MMR proteins have been implicated in homologous recombinational repair. Purified yeast MutSα binds to HJs *in vitro* (Marsischky and Kolodner, 1999), and yeast MutSβ stimulates the activity of the MLH1-MLH3 (MutLγ) endonuclease, which cleaves recombination intermediates in meiosis (Rogacheva et al., 2014). Human MutSβ is required for the efficient HR-mediated repair of DSBs, and deficiencies in *MSH3* result in persistent DNA damage and decreased HR efficiency (Burdova et al., 2015; Franchitto et al., 2003; Park et al., 2013; van Oers et al., 2014). These observations raise the intriguing possibility that interactions between SLX4 and the MMR proteins might also impact upon the resolution of HJs in somatic cells.

In this study, we identify a role for human MutSβ-SLX4 complexes in the cleavage of recombination intermediates. We show that MutSβ binds specifically to HJs *in vitro* and stimulates their cleavage by SLX1-SLX4 and the SMX trinuclease complex. In addition, we show that MutSβ is required for the efficient processing of late recombination intermediates in human cells. We
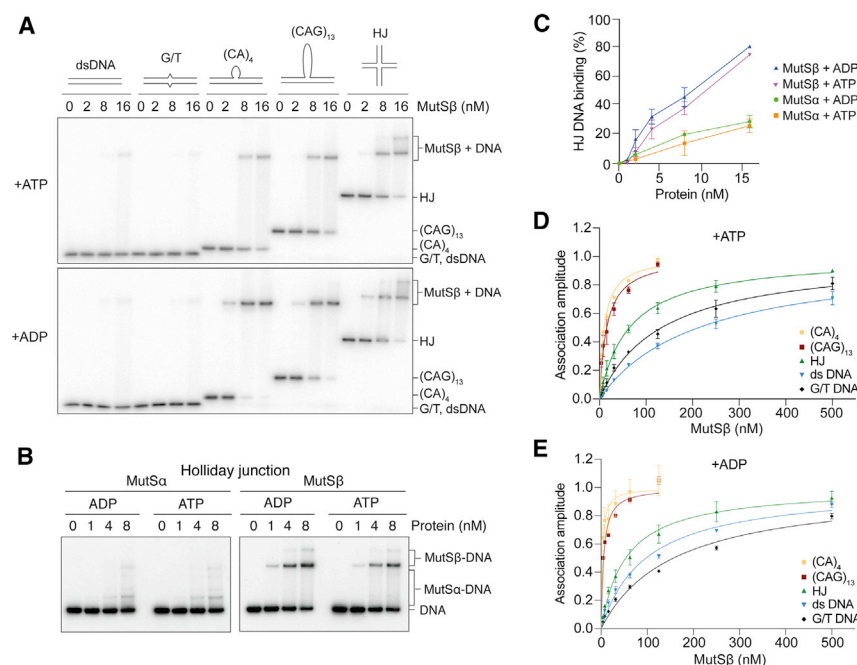
**Figure 2. Specificity of DNA Binding by MutSβ**

(A) MutSβ was incubated with 5′-$^{32}$P-labeled homoduplex DNA (dsDNA) or DNA containing a G/T mismatch, $(CA)_4$ loop, $(CAG)_{13}$ loop, or HJ (3 nM) in the presence of ATP or ADP (1 mM) as indicated, and the products were analyzed by neutral PAGE and autoradiography.

(B) Comparison of Holliday junction (HJ) binding by MutSα or MutSβ. Reactions were carried out as in (A).

(C) Quantification of HJ DNA binding by MutSα or MutSβ. EMSAs were carried out as in (A), and binding is expressed as a percentage of total radiolabeled DNA. Results are displayed as mean ± SD.

(D and E) Normalized equilibrium binding curves for MutSβ binding to the indicated biotinylated DNAs in the presence of ATP or ADP (1 mM), monitored by biolayer interferometry.

Solid lines represent the normalized best fits of the averaged measurement values. Error bars represent SEM.

propose that MutSβ is an important component of the SLX4-repair complex and contributes to its many diverse functions in DNA repair.

## RESULTS

### Interaction of SLX4 with MutSβ

SLX4 protein acts as a scaffold for the targeting and activation of multiple proteins involved in genome stability, telomere maintenance, MMR, and trinucleotide repeat instability (Figure 1A). Mass spectrometry analyses have demonstrated interactions between SLX4 and MSH2, MSH3, and MSH6, and the MSH2-SLX4 interaction has been verified by co-immunoprecipitation and yeast two-hybrid assays (González-Prieto et al., 2015; Svendsen et al., 2009; Zhang et al., 2019). However, little is known about the functions of these interactions or how they contribute to genome stability.

Using the yeast two-hybrid system, we found that SLX4 interacts directly with MSH2 and MSH3, but not MSH6 (Figures 1B and 1C). In these experiments, MUS81 was used as a positive control and GEN1 as a negative control. To determine whether SLX4 interacts with MutSβ within a cellular context, SLX4$_{GFP}$ was transiently expressed in HEK293T cells, and proteins were immunoprecipitated from the cell-free extracts using GFP antibodies. SLX4$_{GFP}$ was found to pull down endogenous MSH2 and MSH3 (MutSβ) (Figure 1D). However, despite there being a 10:1 ratio of MutSα to MutSβ in human cells (Drummond et al., 1997; Marra et al., 1998), we were unable to detect MSH6 in the SLX4$_{GFP}$ immunoprecipitate. These results indicate that SLX4 interacts predominantly with MutSβ, raising the possibility that the SLX4 binding site on MSH3 is important for interaction with SLX4. Alternatively, MutSα-SLX4 interactions may be weak or transient in nature and therefore difficult to detect by pull-down.

As interactions between SLX4 and MUS81-EME1 are enhanced at the onset of mitosis to form the SMX trinuclease complex (Duda et al., 2016; Wyatt et al., 2013), we next determined whether interactions between SLX4 and MutSβ might also be temporally regulated. To do this, SLX4$_{GFP}$ was transiently overexpressed in HeLaK cells, as these cells are amenable to chemical synchronization. Cells were synchronized in early S phase (G1/S) or mitosis (M), and GFP antibodies were used for immunoprecipitation. In contrast to MUS81, which associates with SLX4 only in M phase, endogenous MSH2 was found co-immunoprecipitate with SLX4 at all stages of the cell cycle (Figure S1A). These results indicate that the interaction of SLX4 with MutSβ exhibits no significant temporal regulation.

### MutSβ Binds to Recombination Intermediates *In Vitro*

The interaction of SLX4 with MutSβ, but not MutSα, raises the possibility that MutSβ plays a functional role in reactions mediated by the SMX HJ resolvase. We therefore purified MutSβ (Figure S1B) and investigated whether it binds specifically to HJs *in vitro*. To do this, the interaction of MutSβ with HJs, $(CA)_4$, and $(CAG)_{13}$ heteroduplex loops, DNA containing a single (G/T) mismatch, or homoduplex DNA (double-stranded DNA [dsDNA]), was compared by EMSA. These experiments were carried out in the presence of poly(dI-dC), a competitor that eliminates nonspecific binding. We observed that MutSβ binds HJs with an affinity comparable to heteroduplex loops, its canonical substrate (Figure 2A).

Previously, purified yeast MutSα was shown to bind to HJs *in vitro* (Marsischky et al., 1999). Electrophoretic mobility shift assays (EMSAs) were therefore used to compare the relative affinities of human MutSα and MutSβ for HJs. We found that in comparison to MutSβ, purified MutSα (Figure S1C) showed substantially less binding to HJ DNA (Figures 2B and 2C).
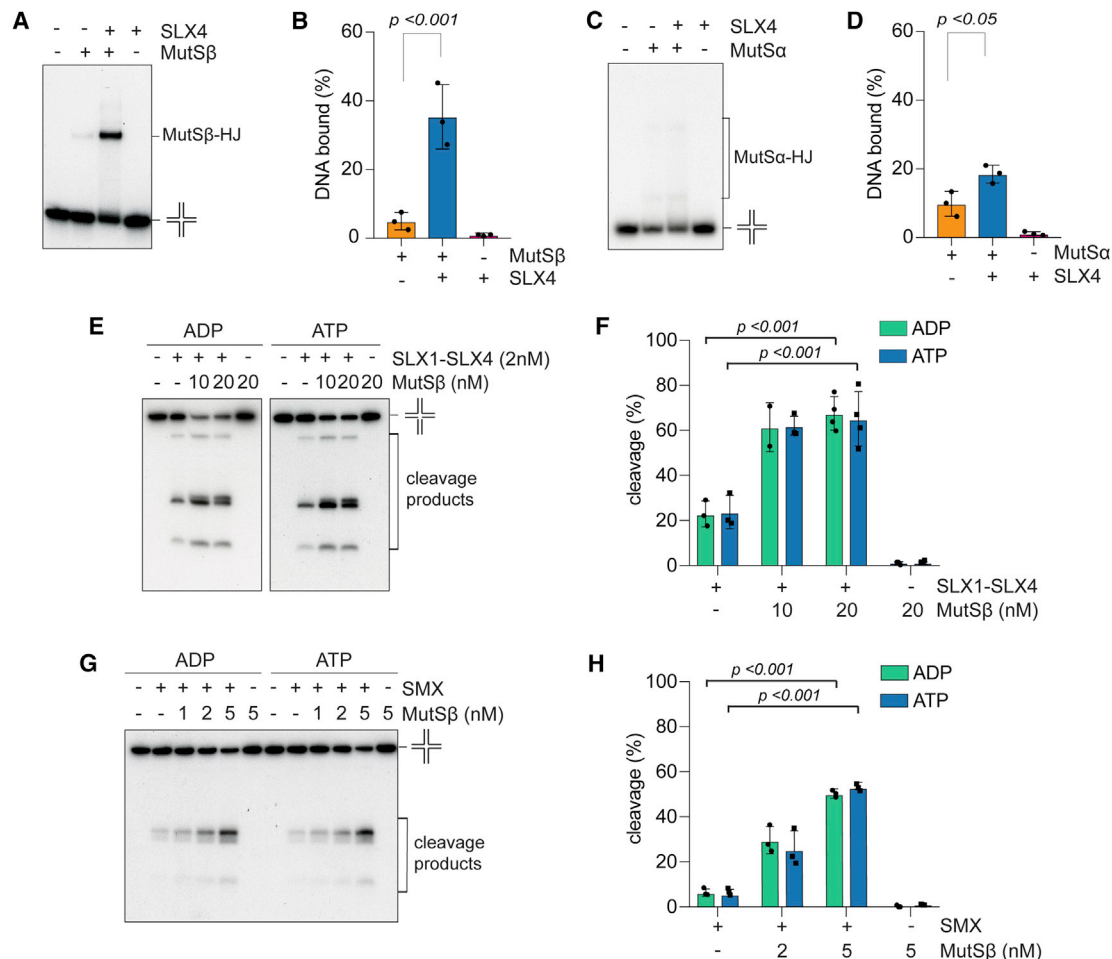
**Figure 3. Cooperation between MutSβ and SLX4 Complexes for HJ Cleavage**

(A) Binding of 5′-$^{32}$P-labeled HJ DNA (3 nM) by MutSβ (4 nM) in the presence or absence of SLX4 (12 nM). Reactions contained ADP (1 mM). Cleavage products were analyzed by neutral PAGE and autoradiography.

(B) Quantification of (A). DNA binding is expressed as a percentage of total radiolabeled DNA. Results are displayed as mean ± SD. Black circles represent individual values.

(C and D) As in (A) and (B), except that reactions were carried out with MutSα (16 nM) and SLX4 (12 nM).

(E) Cleavage of 5′-$^{32}$P-labeled HJ DNA (10 nM) by SLX1-SLX4 (2 nM) in the presence or absence of MutSβ. Reactions contained ADP or ATP (1 mM)

(F) Quantification of (E). DNA cleavage is expressed as a percentage of total radiolabeled DNA. Results are displayed as mean ± SD. Black circles represent individual values.

(G) Cleavage of 5′-$^{32}$P-labeled HJ DNA (10 nM) by SMX (0.1 nM) in the presence or absence of MutSβ. Reactions contained ADP or ATP (1 mM)

(H) Quantification of (G). DNA cleavage is expressed as a percentage of total radiolabeled DNA. Results are displayed as mean ± SD. Black circles represent individual values.

To gain an in-depth understanding of the relative binding affinities of MutSβ for a variety of DNAs, biolayer interferometry (BLI) analyses were conducted (Figures 2D, 2E, and S2; Table S1). Using this approach, ATP-bound MutSβ was found to bind to HJs with an average $K_d$ of 67 ± 18 nM. Although this affinity was lower than that observed with (CA)$_4$ loops and (CAG)$_{13}$ hairpins (10 ± 2 and 18 ± 8, respectively), it was greater than that observed with dsDNA and G/T mismatch structures (213 ± 14 nM and 132 ± 25 nM, respectively). These data indicate that in addition to heteroduplex loop DNAs, MutSβ specifically binds HJs in vitro.

In response to mismatch binding, MutS homologs undergo ATP-dependent conformational changes required for the completion of MMR (Constantin et al., 2005; Habraken et al., 1998; Kadyrov et al., 2006). These changes lead to a marked reduction in DNA binding affinity. For example, ATP-bound MutSβ binds heteroduplex loops, hairpins, and duplex DNA with a lower affinity than ADP-bound MutSβ (Gradia et al., 1999; Iaccarino et al., 2000; Wilson et al., 1999). Consistent with these observations, ATP-bound MutSβ was found to display a ∼4-fold lower affinity than ADP-bound MutSβ for (CA)$_4$ and (CAG)$_{13}$ loops (Figures S2A and S2B; Table S1). A similar dependency on nucleotide state was observed with MutSβ and duplex DNA (Figure S2C; Table S1). These differences, however, were not observed with HJ DNA, as MutSβ bound HJs with a similar
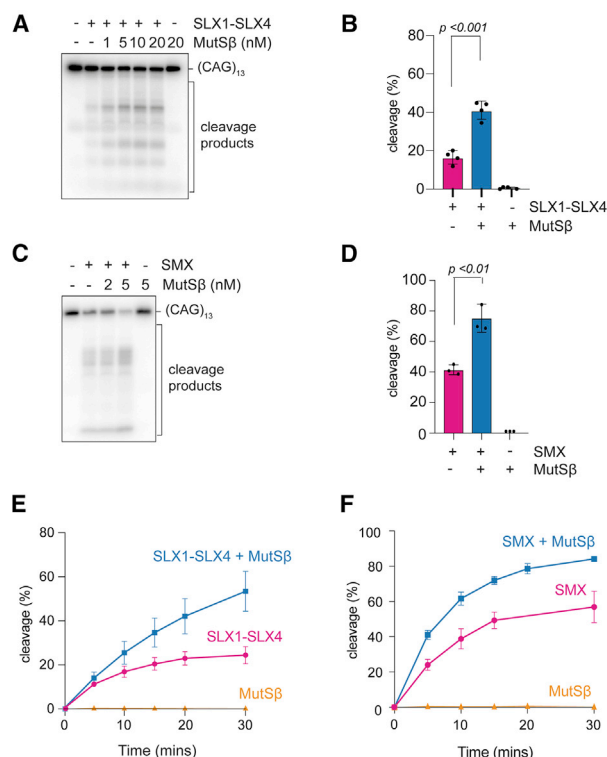
**Figure 4. MutSβ Stimulates Heteroduplex Loop Cleavage by SLX1-SLX4 or SMX**

(A) Cleavage of 5′-$^{32}$P-labeled (CAG)$_{13}$ DNA (10 nM) by SLX1-SLX4 (1.5 nM) in the presence or absence of MutSβ. Reactions contained ATP (1 mM). Cleavage products were analyzed by neutral PAGE and phosphorimaging.

(B) Quantification of (CAG)$_{13}$ DNA cleavage by SLX1-SLX4 (1.5 nM) in the presence or absence of MutSβ (20 nM), as shown in (A). DNA cleavage is expressed as a percentage of total radiolabeled DNA. Results are displayed as mean ± SD. Black circles represent individual values.

(C) Cleavage of 5′-$^{32}$P-labeled (CAG)$_{13}$ DNA (10 nM) by SMX (0.5 nM) in the presence or absence of MutSβ. Reactions contained ATP (1 mM).

(D) Quantification of (CAG)$_{13}$ DNA cleavage, as shown in (C), by SMX (0.5 nM) in the presence or absence of MutSβ (5 nM). DNA cleavage is expressed as a percentage of total radiolabeled DNA. Results are displayed as the mean ± SD. Black circles represent individual values.

(E) Time course of the cleavage of 5′-$^{32}$P-labeled (CAG)$_{13}$ DNA (10 nM) by SMX (0.5 nM) in the presence or absence of MutSβ (5 nM). Reactions were carried out as in (C).

(F) Time course indicating the cleavage of 5′-$^{32}$P-labeled (CAG)$_{13}$ DNA (10 nM) by SMX (0.5 nM) in the presence or absence of MutSβ (5 nM).

affinity in the presence of ATP or ADP (Figures 2A, 2C, and S2D; Table S1). These results indicate that the mode of binding of MutSβ to HJs may differ from that required for heteroduplex loop repair.

## MutSβ Stimulates HJ Cleavage by SLX1-SLX4 and SMX

To determine whether MutSβ and SLX4 cooperate in their interactions with HJs, we next purified SLX4, SLX1-SLX4, and the SMX trinuclease for further *in vitro* analyses (Figures S1D–S1F). First, we investigated any cooperative effects on HJ binding by the combined presence of SLX4 and MutSβ and found that SLX4 greatly stimulated the formation of MutSβ-HJ complexes

(Figures 3A and 3B). We did not, however, observe the formation of a stable tertiary MutSβ-SLX4-DNA complex in the EMSA analyses, indicating that interactions between SLX4 and the MutSβ-DNA complex may be transient. In contrast, SLX4 failed to have a similar effect on the formation of MutSα-HJ complexes (Figures 3C and 3D). As SLX4 interacts only very weakly with MutSα (Figures 1 and S1), these data show that direct MutSβ-SLX4 interactions are likely to be responsible for the stimulation of HJ binding by MutSβ.

Next, we determined whether MutSβ could stimulate HJ resolution by SLX4 complexes *in vitro*. We found that MutSβ significantly increased HJ cleavage by both SLX1-SLX4 (Figures 3E and 3F) and SMX (Figures 3G and 3H). The levels of cleavage were similar in the presence of ADP or ATP. In contrast, MutSα, failed to stimulate HJ cleavage by SLX1-SLX4 (Figures S3A and S3B) and only weakly enhanced cleavage by SMX (Figures S3C and S3D). We also found that MutSβ stimulated the cleavage of (CAG)$_{13}$ heteroduplex loops by either SLX1-SLX4 (Figures 4A, 4B, and 4E) or SMX (Figures 4C, 4D, and 4F), indicating that the cooperation between SLX4 and MutSβ extends beyond HJs to canonical MutSβ substrates. Since these experiments were carried out with small synthetic DNAs, produced by the annealing complementary oligonucleotides, we next determined whether MutSβ might also stimulate the resolution of a HJ contained within a much larger and more physiologically relevant plasmid sized substrate made by RecA-mediated DNA strand exchange (Figure S4A). Again, we found that MutSβ stimulated HJ cleavage by SMX (Figures S4B and S4C). Taken together, these results indicate that MutSβ and SLX4 complexes cooperate in the cleavage of both recombination intermediates and DNA loop structures.

As MutSβ binds specifically to HJs and stimulates their cleavage by SLX4 complexes, we reasoned that MutSβ might facilitate resolution by binding HJs and promoting the recruitment of SLX4 complexes to the DNA. To determine whether direct interactions between SLX4 and MutSβ are necessary for the stimulation of HJ cleavage, we investigated whether MutSβ could enhance HJ cleavage by SLX1 bound to the C-terminal domain of SLX4 (SLX4$^{CCD}$) (Figures S1G–S1I). SLX1-SLX4$^{CCD}$ fails to interact with MutSβ due to deletion of the N-terminal domain that is required for MutSβ interaction (Svendsen et al., 2009) (Figure 5A) but retains nuclease activity that can facilitate HJ cleavage *in vitro* (Gaur et al., 2015; Gaur et al., 2019). We found that unlike full-length SLX4, SLX1-SLX4$^{CCD}$ failed to stimulate the binding of MutSβ to HJs (Figures 5B and 5C). Also, in contrast to full-length SLX1-SLX4, HJ cleavage by SLX1-SLX4$^{CCD}$ was not stimulated by the presence of MutSβ (Figures 5D–5F). These results show that direct interactions between SLX4 and MutSβ are required for their cooperation in HJ binding and cleavage.

## MutSβ Is Required for Efficient SCE in BLM-Deficient Cells

The cellular efficiency of HJ resolution can be determined by measuring the incidence of SCEs in metaphase chromosomes in BLM-deficient GM08505 cells. As BLM is required for dissolution of HJs, GM08505 cells are only able to process HJs by SMX/GEN1-mediated resolution, resulting in a high frequency of SCEs (Wechsler et al., 2011; Wu and Hickson, 2003). To determine
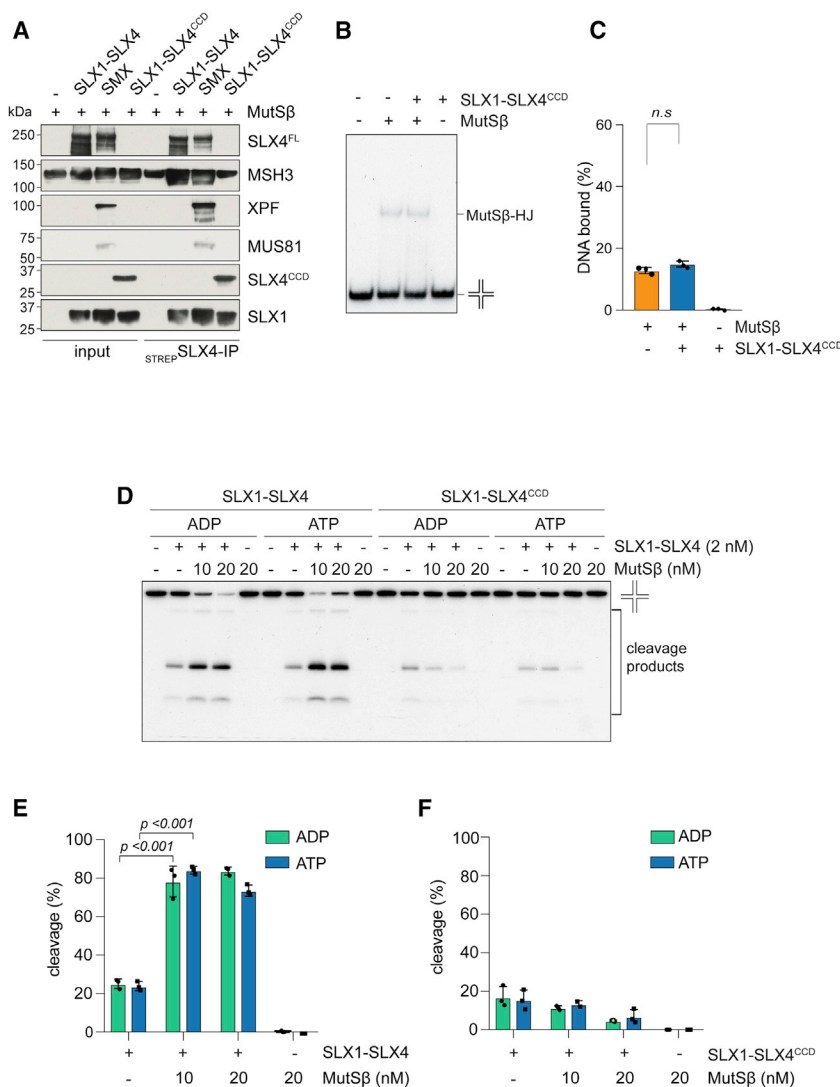
**Figure 5. Interactions between SLX4 and MutSβ Are Necessary for HJ Cleavage**

(A) Strep-pull-down reactions containing $_{HIS}$MutSβ in the presence or absence of $_{STREP}$SLX4 complexes (SLX1-$_{STREP}$SLX4, $_{STREP}$SMX, or SLX1-$_{STREP}$SLX4$^{CCD}$). Proteins were detected by immunoblotting.

(B) Binding of 5′-$^{32}$P-labeled HJ DNA (3 nM) by MutSβ (4 nM) in the presence or absence of SLX1-SLX4$^{CCD}$ (12 nM). Reactions contained EDTA (5 mM) to prevent HJ cleavage by SLX1-SLX4$^{CCD}$. Cleavage products were analyzed by neutral PAGE and autoradiography.

(C) Quantification of (B). DNA binding is expressed as a percentage of total radiolabeled DNA. Results are displayed as mean ± SD. Black circles represent individual values.

(D) Cleavage of 5′-$^{32}$P-labeled HJ DNA by SLX1-SLX4 or SLX1-SLX4$^{CCD}$ in the presence or absence of MutSβ. Reactions contained ADP or ATP (1 mM). Products were analyzed by neutral PAGE and autoradiography.

(E and F) Quantification of the data shown in (B). DNA cleavage is expressed as a percentage of total radiolabeled DNA. Results are displayed as mean ± SD. Black circles represent individual values.

contrast to HR-UFBs, FS-UFBs are characterized by the presence of FANCD2 repair foci at either end of the replication protein A (RPA)-coated ssDNA bridge (Figure 7A).

To determine whether loss of MutSβ leads to mitotic defects, WT and $GEN1^{-/-}$ T-REx-293 cells were treated with siRNA-depleting MSH3, MSH6, or SLX4 (Figure S6), and anaphase cells containing HR-UFBs or FS-UFBs were analyzed and quantified (Figures 7B–7D). These experiments were carried out in the absence of any exogenous DNA-damaging agents that would induce increased UFB formation (Chan et al., 2018). Wild-type (WT) cells treated with siMSH3 displayed a significant increase in the incidence of HR-UFBs. Treatment with siMSH6 did not induce HR-UFBs (Figure 7C). These results are consistent with our biochemical observations, indicating that MutSβ plays a role in the cleavage of HJs in unperturbed human cells.

As expected, $GEN1^{-/-}$ cells exhibited an elevated level of HR-UFB formation, and these levels increased further following treatment with MSH3 siRNA (Figure 7C). These results are consistent with our SCE analyses indicating that GEN1 and MSH3 act in different pathways of HJ resolution. Moreover, we found that cells treated with siRNAs against MSH3 and SLX4 were epistatic for HR-UFB formation, indicating that MutSβ-SLX4 complexes cooperate to cleave recombination intermediates.

The levels of replication-based FS-UFBs were also determined under the same conditions (Figure 7D). In WT cells, siRNA against MSH3, MSH6, or SLX4 had no effect on the incidence of FS-UFBs. However, siRNA-mediated depletion of MSH3 from

whether MutSβ plays a cellular role in HJ resolution, we therefore treated GM08505 cells with small interfering RNA (siRNA) against MSH3, MSH6, SLX4, and GEN1 (Figure S5) and measured SCE formation. The frequency of SCE formation was found to be reduced by siRNAs against MSH3, SLX4, or GEN1, but not by MSH6 siRNA (Figure 6). Consistent with a role for MutSβ in SMX-mediated HJ resolution, we found that the observed reduction in SCE formation by MSH3 siRNA was epistatic with SLX4, but not with GEN1 (Figure 6).

### HJ Resolution by MutSβ-SLX4 Complexes Prevent Mitotic Defects and DNA Damage

Previous studies have shown that HJ resolution defects manifest in the formation of RPA-coated single-stranded DNA (ssDNA) HR ultrafine bridges (HR-UFBs) that can be visualized at anaphase. HR-UFBs arise at high frequency in cells lacking SMX and GEN1, and are distinct from UFBs generated as a result of incomplete replication of genomic regions such as CFSs (fragile site UFBs [FS-UFBs]) (Chan et al., 2009; Chan et al., 2018). In

**A**



**B**



**Figure 6. Contribution of MutSβ to SCEs in Bloom's Syndrome Cells**
(A) Representative images of metaphase spread prepared from Bloom's-deficient GM08505 cells, treated with the indicated siRNAs. Scale bars represents 10 μm.
(B) Quantification of SCE frequency. Each data point represents one metaphase/cell.

$GEN1^{-/-}$ cells resulted in a significant increase in FS-UFBs. Increased FS-UFB formation was also observed following depletion of SLX4. These results indicate that loss of MSH3 or SLX4 from $GEN1^{-/-}$ cells leads to the formation of unresolved DNA replication intermediates that persist until mitosis.

Finally, we determined the cellular consequences of inefficient HJ resolution in the absence of MutSβ. To do this, WT and $GEN1^{-/-}$ T-REx-293 cells were treated with siRNA-depleting MSH3, MSH6, or SLX4 (Figure S6). Cells were treated with cisplatin to induce an increased load of HR intermediates, and DNA damage was measured in the following G1 phase by measuring the formation of MDC1 foci in cyclin-A-negative cells (Figures 7E and 7F). Consistent with our HR-UFB analysis, cells treated with siMSH3, but not siMSH6, displayed a small but significant increase in MDC1 foci. The increase was found to be epistatic with SLX4, but not with GEN1, indicating that HJ resolution by SLX4-MutSβ complexes is required to prevent DNA damage.

Taken together, these data are consistent with a role for MutSβ-SLX4 complexes in safeguarding genomic integrity by cleaving recombination and replication intermediates to allow accurate sister chromatid separation.

## DISCUSSION

SLX4 acts as a scaffold for the assembly of three SSEs involved in DNA replication, recombination, and repair. These SLX4-associated SSEs promote the cleavage of ICLs, maintain telomere length, and resolve recombination and replication intermediates. SLX4 therefore provides the platform for a vital molecular toolkit that safeguards genomic integrity.

The SLX4 toolkit is targeted to specific regions of the genome by interactions with other proteins. For example, SLX4 interacts with TRF2 and SLX4IP, two telomere binding proteins, to regulate telomere length in ALT (alternative lengthening of telomeres) cells (Panier et al., 2019; Sarkar et al., 2015; Sobinoff et al., 2017; Svendsen et al., 2009; Wan et al., 2013; Wilson et al., 2013; Zhang et al., 2019). In addition, interactions between SLX4, XPF-ERCC1, and SLX4IP are required for the efficient repair of DNA ICLs (Hashimoto et al., 2015; Hoogenboom et al., 2019; Kim et al., 2013; Zhang et al., 2019). Recently, it was shown that SLX4 interacts with RTEL1, and this interaction helps overcome encounters between the replisome and transcription machinery, particularly in regions of the genome that exhibit replication/transcription stress (Takedachi et al., 2020; Wu et al., 2020). These regions include those that form R-loops and G4 quadraplex structures. Remarkably, cancer-associated mutations in *SLX4* and germline mutations in *RTEL1* that cause Hoyeraal-Hreidarsson syndrome were defective in SLX4-RTEL1 interactions (Takedachi et al., 2020).

Here, we have shown that MutSβ binds HJs and stimulates the resolution of recombination intermediates by both SLX1-SLX4 and the SMX complex. Stimulation was dependent upon a direct interaction between MutSβ and SLX4, as we failed to see increased cleavage activity when SLX1-SLX4$^{CCD}$ nuclease was analyzed in the presence of MutSβ. This nuclease, containing only the C-terminal SLX1-interacting domain of SLX4, is as active as full-length SLX1-SLX4 but is unable to interact with MutSβ. Consistent with our biochemical studies, cells defective for *MSH3* exhibited reduced SCE formation and an increased frequency of HR-UFBs, characteristic of a defect in the resolution of recombination intermediates. In addition, $GEN1^{-/-}$ cells depleted for MSH3 exhibited increased FS-UFB formation, indicating that the MutSβ-SMX complex plays a dual role in the resolution of both recombination and late replication intermediates. We also found that MutSβ stimulated the nucleolytic cleavage of heteroduplex loop structures by SLX1-SLX4 or SMX, suggesting that MutSβ-SMX may provide an alternative, or backup, loop-processing pathway to that offered by MutSβ-MutLα. At the present time, however, we have no cellular data to support this hypothesis.

In the presence of $Mg^{2+}$, HJs adopt a stacked X-structure with pairwise coaxial stacking of the helical arms (Duckett et al., 1988, 1990; Eichman et al., 2000). These structures are bound with a high affinity by MutSβ. Previously, the crystal structure of human MutSβ bound to a small heteroduplex loop revealed that a Lys-Tyr motif in the mismatch binding domain (MBD) of MSH3 interacts with phosphate groups in the DNA (Gupta et al., 2011). MutSα on the other hand, interacts with a G/T mismatch using a conserved Phe residue in the MBD of MSH6 that makes specific base contacts (Warren et al., 2007). Consequently, MutSβ binds to heteroduplex DNA with a wider range of bending angles than MutSα. While the precise mechanism of HJ binding by MutSβ is unknown and will require further biochemical and structural analyses, these differences may explain why MutSβ binds HJs with a higher efficiency than MutSα.
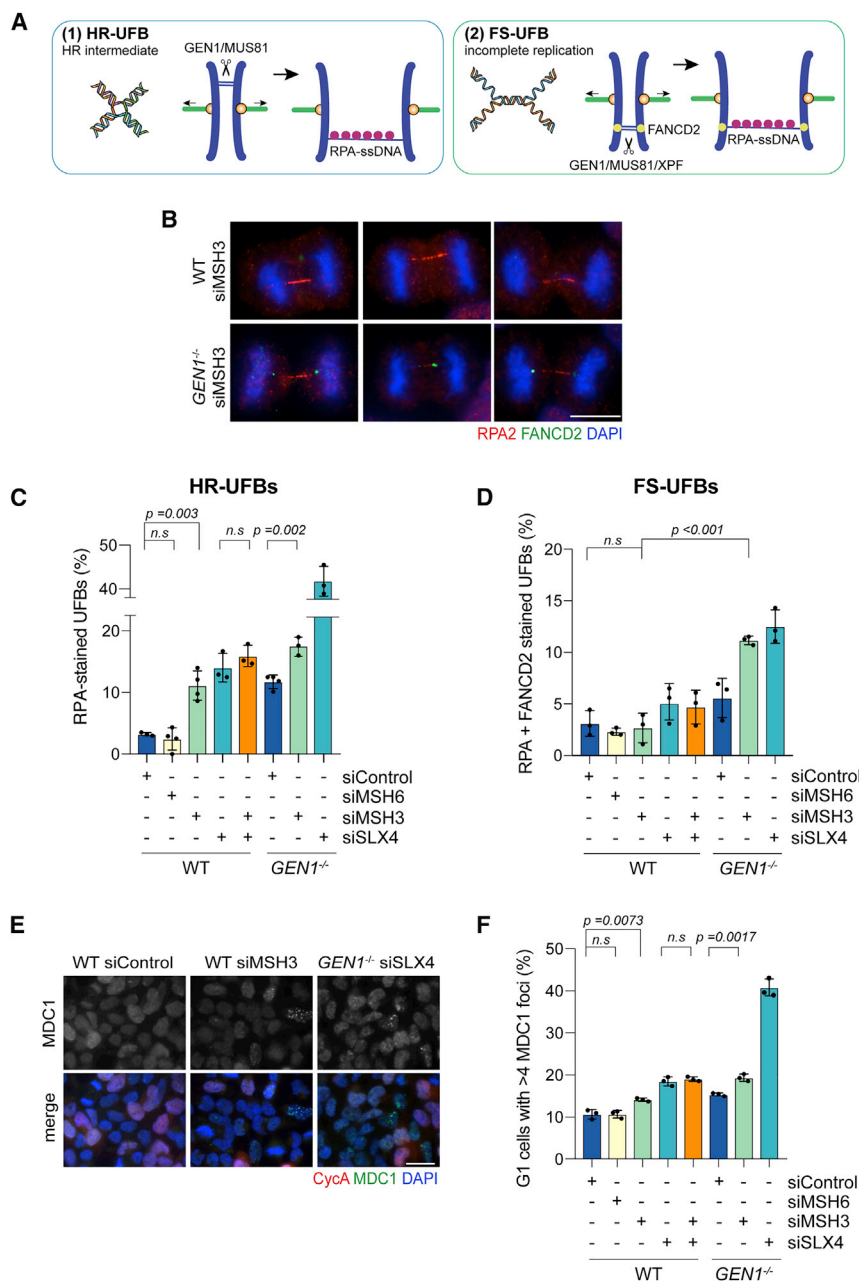
**Figure 7. Loss of MutSβ Leads to Increased Incidence of DNA UFBs in Mitosis and Damage in G1**

(A) Schematic diagram showing recombination (HR) and replication-stress-induced fragile site (FS) DNA ultrafine bridges (UFBs) that occur during anaphase. HR-UFBs are RPA-coated ssDNA and not flanked by FANCD2 repair foci. FS-UFBs are RPA-coated ssDNA and are flanked by twin FANCD2 repair foci. UFBs are normally cleaved by SMX or GEN1.

(B) Representative images of mitotic WT or $GEN1^{-/-}$ T-REx-293 cells treated with the indicated siRNAs. Anaphases containing FANCD2-negative HR-UFBs and FANCD2-positive FS-UFBs are shown. Nuclear DNA and UFBs were visualized by DAPI and RPA staining, respectively. Images are of a single z-plane. Scale bar represents 10 μm.

(C and D) Quantification of cells (40–60 per condition) with FANCD2-negative HR-UFBs or FANCD2-flanked UFBs in WT or $GEN1^{-/-}$ T-REx-293 cells treated with MSH3, MSH6, or SLX4 siRNAs.

(E) Representative images of WT or $GEN1^{-/-}$ T-REx-293 cells treated with the indicated siRNAs. Cells were treated with cisplatin (1 μM) and then released into fresh media. Nuclear DNA, MDC1, and cyclin A were detected using DAPI, anti-MDC1, and anti-cyclin A antibodies, respectively. Scale bar represents 20 μm.

(F) Quantification of cyclin-A-negative G1 cells (60–80 per condition) with >4 MDC1 foci in WT or $GEN1^{-/-}$ T-REx-293 cells treated with MSH3, MSH6, or SLX4 siRNAs.

It is known that the composition of SLX4 complexes changes throughout the cell cycle. Whereas SLX1-SLX4 and XPF-ERCC1 form a constitutive complex, the interaction of SLX4 with MUS81-EME1 is dependent upon CDK1/PLK1 phosphorylation events that occur at prometaphase. As such, replication forks are protected in S phase, and the processing of recombination intermediates and late-replicating intermediates is restricted to mitosis. We found that MutSβ-SLX4 interactions occur regardless of cell-cycle stage and that MutSβ stimulated HJ processing by both the constitutive nuclease SLX1-SLX4 and the mitosis-specific SMX trinuclease complex. These results lead us to propose that MutSβ is an integral component of the SLX4 repair toolkit and may modulate the activity of this complex toward DNA intermediates that arise in multiple genomic contexts. For example, during replication, SLX4-associated SSEs are required to cleave HJs that form during the restart of collapsed replication forks (Fugger et al., 2013; Garner et al., 2013; Lemaçon et al., 2017) and as a consequence of ICL repair (Castor et al., 2013; Kim et al., 2013; McPherson et al., 2004). MutSβ and SLX4 are both present at active replisomes (Dungrawala et al., 2015; Haye and Gammie, 2015) and independently confer resistance to chemical agents that induce ICL damage

The interaction of MutS homologs with MMR lesions involves an ADP/ATP switch by which substrate recognition causes an ATP-dependent conformational change, leading to reduced binding affinity and higher processivity on DNA (Gradia et al., 1999, 2000; Lang et al., 2011; Wilson et al., 1999). These conformational changes are required for the activation of MutLα and the completion of MMR (Constantin et al., 2005; Kadyrov et al., 2006). However, we find that the binding affinity of MutSβ to HJs and the stimulation of their cleavage by SLX4 complexes are insensitive to the presence of ATP or ADP. These results contrast with the role of MutSβ in heteroduplex loop repair in which MutSβ acts as a sliding clamp that facilitates MutLα action.

and replication stress (Burdova et al., 2015; Kim et al., 2011, 2013; Svendsen et al., 2009; Takahashi et al., 2011). HJs also arise at telomeres in telomerase-negative ALT cells where SLX4 complexes (involving TRF2 and SLX4IP) regulate telomere length by resolving HJs (Panier et al., 2019; Sarkar et al., 2015; Sobinoff et al., 2017; Wan et al., 2013). Consistent with a role for MutSβ-SLX4 in HJ processing at telomeres, it has been shown that siRNA-mediated depletion of MSH2 from ALT cells leads to a reduction in the number of telomeric SCEs (T-SCEs) (Martinez et al., 2017). Finally, in mitosis, the SMX trinuclease complex acts to efficiently resolve residual HJs to allow accurate sister chromatid separation (Chan et al., 2018; Wyatt et al., 2017). Here, we have shown that MutSβ promotes the efficient processing of residual HJs that persist into mitosis by enhancing the recruitment of the SMX repair toolkit. As the inefficient resolution of recombination intermediates is a potential driver of chromosomal instability (Chan et al., 2018; Wechsler et al., 2011), it is possible that MutSβ-SLX4 interactions are particularly relevant in tumors that display hyperactive recombination (Prakash et al., 2015).

Interestingly, not all functions of MutSβ are genome protective. MutSβ plays a critical role in promoting the pathogenic expansion of CAG/CTG trinucleotide repeat tracts in mouse and human cells (Dragileva et al., 2009; Du et al., 2013; Gannon et al., 2012; Keogh et al., 2017; Savouret et al., 2003). Instability of these repeat regions is causative of multiple degenerative disorders, including Huntington's disease and myotonic dystrophy (Iyer et al., 2015). As these diseases do not yet have effective curative treatments, understanding exactly how MutSβ mediates expansion of these regions could provide a key to uncovering new therapeutic avenues. We and others have shown that MutSβ binds specifically to oligonucleotides containing trinucleotide repeats *in vitro* (Owen et al., 2005; Pluciennik et al., 2013; Tian et al., 2009), and heteroduplex loops have been detected in myotonic dystrophy patient tissues with a frequency that positively correlates with their observed instability (Axford et al., 2013). Our observation that MutSβ also stimulates the cleavage of trinucleotide repeat loops by SLX1-SLX4 or SMX indicates that MutSβ-SLX4 complexes may provide additional pathways that contribute to the pathogenic expansion of trinucleotide repeat regions. Further analysis of the interplay between MutSβ and SLX4 should shed new insights into the pathways of both HJ resolution and MMR-mediated heteroduplex loop instability.

## STAR★METHODS

Detailed methods are provided in the online version of this paper and include the following:

## AUTHOR CONTRIBUTIONS

Conceptualization, S.J.Y. and S.C.W.; Investigation, S.J.Y., M.S., R.S.P., M.L., and L.M.; Methodology, S.J.Y., M.S., R.S.P., M.L., L.M., M.C.R.-B., and C.-C.L.; Writing – Original Draft, S.J.Y. and S.C.W.; Funding Acquisition, S.C.W.; Supervision, S.C.W.

## REFERENCES

Acharya, S., Wilson, T., Gradia, S., Kane, M.F., Guerrette, S., Marsischky, G.T., Kolodner, R., and Fishel, R. (1996). hMSH2 forms specific mispair-binding complexes with hMSH3 and hMSH6. Proc. Natl. Acad. Sci. USA *93*, 13629–13634.

Alani, E. (1996). The *Saccharomyces cerevisiae* Msh2 and Msh6 proteins form a complex that specifically binds to duplex oligonucleotides containing mismatched DNA base pairs. Mol. Cell. Biol. *16*, 5604–5615.

Axford, M.M., Wang, Y.H., Nakamori, M., Zannis-Hadjopoulos, M., Thornton, C.A., and Pearson, C.E. (2013). Detection of slipped-DNAs at the trinucleotide

repeats of the myotonic dystrophy type I disease locus in patient tissues. PLoS Genet. *9*, e1003866.

Bogliolo, M., Schuster, B., Stoepker, C., Derkunt, B., Su, Y., Raams, A., Trujillo, J.P., Minguillón, J., Ramírez, M.J., Pujol, R., et al. (2013). Mutations in *ERCC4*, encoding the DNA-repair endonuclease XPF, cause Fanconi anemia. Am. J. Hum. Genet. *92*, 800–806.

Burdova, K., Mihaljevic, B., Sturzenegger, A., Chappidi, N., and Janscak, P. (2015). The mismatch binding factor MutSβ can mediate ATR activation in response to DNA double strand breaks. Mol. Cell *59*, 603–614.

Castor, D., Nair, N., Déclais, A.C., Lachaud, C., Toth, R., Macartney, T.J., Lilley, D.M.J., Arthur, J.S., and Rouse, J. (2013). Cooperative control of Holliday junction resolution and DNA repair by the SLX1 and MUS81-EME1 nucleases. Mol. Cell *52*, 221–233.

Chaganti, R.S., Schonberg, S., and German, J. (1974). A manyfold increase in sister chromatid exchanges in Bloom's syndrome lymphocytes. Proc. Natl. Acad. Sci. USA *71*, 4508–4512.

Chan, Y.W., and West, S.C. (2014). Spatial control of the GEN1 Holliday junction resolvase ensures genome stability. Nat. Commun. *5*, 4844.

Chan, Y.W., and West, S. (2015). GEN1 promotes Holliday junction resolution by a coordinated nick and counter-nick mechanism. Nucleic Acids Res. *43*, 10882–10892.

Chan, K.L., Palmai-Pallag, T., Ying, S., and Hickson, I.D. (2009). Replication stress induces sister-chromatid bridging at fragile site loci in mitosis. Nat. Cell Biol. *11*, 753–760.

Chan, Y.W., Fugger, K., and West, S.C. (2018). Unresolved recombination intermediates lead to a novel class of ultra-fine bridges, chromosome breaks and aberrations. Nat. Cell Biol. *20*, 92–103.

Constantin, N., Dzantiev, L., Kadyrov, F.A., and Modrich, P. (2005). Human mismatch repair: reconstitution of a nick-directed bidirectional reaction. J. Biol. Chem. *280*, 39752–39761.

Crossan, G.P., and Patel, K.J. (2012). The Fanconi anaemia pathway orchestrates incisions at sites of crosslinked DNA. J. Pathol. *226*, 326–337.

Crossan, G.P., van der Weyden, L., Rosado, I.V., Langevin, F., Gaillard, P.H.L., McIntyre, R.E., Gallagher, F., Kettunen, M.I., Lewis, D.Y., Brindle, K., et al.; Sanger Mouse Genetics Project (2011). Disruption of mouse *Slx4*, a regulator of structure-specific nucleases, phenocopies Fanconi anemia. Nat. Genet. *43*, 147–152.

Dehé, P.M., and Gaillard, P.H.L. (2017). Control of structure-specific endonucleases to maintain genome stability. Nat. Rev. Mol. Cell Biol. *18*, 315–330.

Dragileva, E., Hendricks, A., Teed, A., Gillis, T., Lopez, E.T., Friedberg, E.C., Kucherlapati, R., Edelmann, W., Lunetta, K.L., MacDonald, M.E., and Wheeler, V.C. (2009). Intergenerational and striatal CAG repeat instability in Huntington's disease knock-in mice involve different DNA repair genes. Neurobiol. Dis. *33*, 37–47.

Drummond, J.T., Genschel, J., Wolf, E., and Modrich, P. (1997). DHFR/MSH3 amplification in methotrexate-resistant cells alters the hMutSα/hMutSβ ratio and reduces the efficiency of base-base mismatch repair. Proc. Natl. Acad. Sci. USA *94*, 10144–10149.

Drummond, J.T., Li, G.-M., Longley, M.J., and Modrich, P. (1995). Mismatch recognition by an hMSH2-GTBP heterodimer and differential repair defects in tumor cells. Science *268*, 1909–1912.

Du, J., Campau, E., Soragni, E., Jespersen, C., and Gottesfeld, J.M. (2013). Length-dependent CTG·CAG triplet-repeat expansion in myotonic dystrophy patient-derived induced pluripotent stem cells. Hum. Mol. Genet. *22*, 5276–5287.

Duckett, D.R., Murchie, A.I.H., Diekmann, S., von Kitzing, E., Kemper, B., and Lilley, D.M.J. (1988). The structure of the Holliday junction, and its resolution. Cell *55*, 79–89.

Duckett, D.R., Murchie, A.I.H., and Lilley, D.M.J. (1990). The role of metal ions in the conformation of the four-way DNA junction. EMBO J. *9*, 583–590.

Duda, H., Arter, M., Gloggnitzer, J., Teloni, F., Wild, P., Blanco, M.G., Altmeyer, M., and Matos, J. (2016). A mechanism for controlled breakage of under-replicated chromosomes during mitosis. Dev. Cell *39*, 740–755.

Dungrawala, H., Rose, K.L., Bhat, K.P., Mohni, K.N., Glick, G.G., Couch, F.B., and Cortez, D. (2015). The replication checkpoint prevents two types of fork collapse without regulating replisome stability. Mol. Cell *59*, 998–1010.

Duraturo, F., Liccardo, R., De Rosa, M., and Izzo, P. (2019). Genetics, diagnosis and treatment of Lynch syndrome: old lessons and current challenges. Oncol. Lett. *17*, 3048–3054.

Eichman, B.F., Vargason, J.M., Mooers, B.H.M., and Ho, P.S. (2000). The Holliday junction in an inverted repeat DNA sequence: sequence effects on the structure of four-way junctions. Proc. Natl. Acad. Sci. USA *97*, 3971–3976.

Fekairi, S., Scaglione, S., Chahwan, C., Taylor, E.R., Tissier, A., Coulon, S., Dong, M.Q., Ruse, C., Yates, J.R., 3rd, Russell, P., et al. (2009). Human SLX4 is a Holliday junction resolvase subunit that binds multiple DNA repair/recombination endonucleases. Cell *138*, 78–89.

Fishel, R. (2015). Mismatch repair. J. Biol. Chem. *290*, 26395–26403.

Fishel, R., Lescoe, M.K., Rao, M.R.S., Copeland, N.G., Jenkins, N.A., Garber, J., Kane, M., and Kolodner, R. (1993). The human mutator gene homolog *MSH2* and its association with hereditary nonpolyposis colon cancer. Cell *75*, 1027–1038.

Fitzgerald, D.J., Berger, P., Schaffitzel, C., Yamada, K., Richmond, T.J., and Berger, I. (2006). Protein complex expression by using multigene baculoviral vectors. Nat. Methods *3*, 1021–1032.

Franchitto, A., Pichierri, P., Piergentili, R., Crescenzi, M., Bignami, M., and Palitti, F. (2003). The mammalian mismatch repair protein MSH2 is required for correct MRE11 and RAD51 relocalization and for efficient cell cycle arrest induced by ionizing radiation in G2 phase. Oncogene *22*, 2110–2120.

Fugger, K., Chu, W.K., Haahr, P., Kousholt, A.N., Beck, H., Payne, M.J., Hanada, K., Hickson, I.D., and Sørensen, C.S. (2013). FBH1 co-operates with MUS81 in inducing DNA double-strand breaks and cell death following replication stress. Nat. Commun. *4*, 1423.

Gannon, A.M.M., Frizzell, A., Healy, E., and Lahue, R.S. (2012). MutSβ and histone deacetylase complexes promote expansions of trinucleotide repeats in human cells. Nucleic Acids Res. *40*, 10324–10333.

Garner, E., Kim, Y., Lach, F.P., Kottemann, M.C., and Smogorzewska, A. (2013). Human GEN1 and the SLX4-associated nucleases MUS81 and SLX1 are essential for the resolution of replication-induced Holliday junctions. Cell Rep. *5*, 207–215.

Gaur, V., Wyatt, H.D.M., Komorowska, W., Szczepanowski, R.H., de Sanctis, D., Gorecka, K.M., West, S.C., and Nowotny, M. (2015). Structural and mechanistic analysis of the SLX1-SLX4 endonuclease. Cell Rep. *10*, 1467–1476.

Gaur, V., Ziajko, W., Nirwal, S., Szlachcic, A., Gapińska, M., and Nowotny, M. (2019). Recognition and processing of branched DNA substrates by Slx1-Slx4 nuclease. Nucleic Acids Res. *47*, 11681–11690.

Genschel, J., Littman, S.J., Drummond, J.T., and Modrich, P. (1998). Isolation of MutSβ from human cells and comparison of the mismatch repair specificities of MutSβ and MutSα. J. Biol. Chem. *273*, 19895–19901.

German, J. (1993). Bloom syndrome: a mendelian prototype of somatic mutational disease. Medicine (Baltimore) *72*, 393–406.

González-Prieto, R., Cuijpers, S.A., Luijsterburg, M.S., van Attikum, H., and Vertegaal, A.C. (2015). SUMOylation and PARylation cooperate to recruit and stabilize SLX4 at DNA damage sites. EMBO Rep. *16*, 512–519.

Gradia, S., Acharya, S., and Fishel, R. (1997). The human mismatch recognition complex hMSH2-hMSH6 functions as a novel molecular switch. Cell *91*, 995–1005.

Gradia, S., Subramanian, D., Wilson, T., Acharya, S., Makhov, A., Griffith, J., and Fishel, R. (1999). hMSH2-hMSH6 forms a hydrolysis-independent sliding clamp on mismatched DNA. Mol. Cell *3*, 255–261.

Gradia, S., Acharya, S., and Fishel, R. (2000). The role of mismatched nucleotides in activating the hMSH2-hMSH6 molecular switch. J. Biol. Chem. *275*, 3922–3930.

Guervilly, J.H., and Gaillard, P.H. (2018). SLX4: multitasking to maintain genome stability. Crit. Rev. Biochem. Mol. Biol. *53*, 475–514.

Gupta, S., Gellert, M., and Yang, W. (2011). Mechanism of mismatch recognition revealed by human MutSβ bound to unpaired DNA loops. Nat. Struct. Mol. Biol. *19*, 72–78.

Habraken, Y., Sung, P., Prakash, L., and Prakash, S. (1998). ATP-dependent assembly of a ternary complex consisting of a DNA mismatch and the yeast MSH2-MSH6 and MLH1-PMS1 protein complexes. J. Biol. Chem. *273*, 9837–9841.

Hashimoto, K., Wada, K., Matsumoto, K., and Moriya, M. (2015). Physical interaction between SLX4 (FANCP) and XPF (FANCQ) proteins and biological consequences of interaction-defective missense mutations. DNA Repair (Amst.) *35*, 48–54.

Haye, J.E., and Gammie, A.E. (2015). The eukaryotic mismatch recognition complexes track with the replisome during DNA synthesis. PLoS Genet. *11*, e1005719.

Hodskinson, M.R.G., Silhan, J., Crossan, G.P., Garaycoechea, J.I., Mukherjee, S., Johnson, C.M., Schärer, O.D., and Patel, K.J. (2014). Mouse SLX4 is a tumor suppressor that stimulates the activity of the nuclease XPF-ERCC1 in DNA crosslink repair. Mol. Cell *54*, 472–484.

Holloway, J.K., Mohan, S., Balmus, G., Sun, X., Modzelewski, A., Borst, P.L., Freire, R., Weiss, R.S., and Cohen, P.E. (2011). Mammalian BTBD12 (SLX4) protects against genomic instability during mammalian spermatogenesis. PLoS Genet. *7*, e1002094.

Hoogenboom, W.S., Boonen, R.A.C.M., and Knipscheer, P. (2019). The role of SLX4 and its associated nucleases in DNA interstrand crosslink repair. Nucleic Acids Res. *47*, 2377–2388.

Hou, C., Chan, N.L., Gu, L., and Li, G.M. (2009). Incision-dependent and error-free repair of (CAG)(n)/(CTG)(n) hairpins in human cell extracts. Nat. Struct. Mol. Biol. *16*, 869–875.

Iaccarino, I., Marra, G., Dufner, P., and Jiricny, J. (2000). Mutation in the magnesium binding site of hMSH6 disables the hMutSα sliding clamp from translocating along DNA. J. Biol. Chem. *275*, 2080–2086.

Iaccarino, I., Palombo, F., Drummond, J., Totty, N.F., Hsuan, J.J., Modrich, P., and Jiricny, J. (1996). MSH6, a *Saccharomyces cerevisiae* protein that binds to mismatches as a heterodimer with MSH2. Curr. Biol. *6*, 484–486.

Ip, S.C.Y., Rass, U., Blanco, M.G., Flynn, H.R., Skehel, J.M., and West, S.C. (2008). Identification of Holliday junction resolvases from humans and yeast. Nature *456*, 357–361.

Iyer, R.R., Pluciennik, A., Napierala, M., and Wells, R.D. (2015). DNA triplet repeat expansion and mismatch repair. Annu. Rev. Biochem. *84*, 199–226.

Kadyrov, F.A., Dzantiev, L., Constantin, N., and Modrich, P. (2006). Endonucleolytic function of MutLα in human mismatch repair. Cell *126*, 297–308.

Keogh, N., Chan, K.Y., Li, G.M., and Lahue, R.S. (2017). MutSβ abundance and Msh3 ATP hydrolysis activity are important drivers of CTG•CAG repeat expansions. Nucleic Acids Res. *45*, 10068–10078.

Kim, Y., Lach, F.P., Desetty, R., Hanenberg, H., Auerbach, A.D., and Smogorzewska, A. (2011). Mutations of the *SLX4* gene in Fanconi anemia. Nat. Genet. *43*, 142–146.

Kim, Y., Spitz, G.S., Veturi, U., Lach, F.P., Auerbach, A.D., and Smogorzewska, A. (2013). Regulation of multiple DNA repair pathways by the Fanconi anemia protein SLX4. Blood *121*, 54–63.

Lang, W.H., Coats, J.E., Majka, J., Hura, G.L., Lin, Y., Rasnik, I., and McMurray, C.T. (2011). Conformational trapping of mismatch recognition complex MSH2/MSH3 on repair-resistant DNA loops. Proc. Natl. Acad. Sci. USA *108*, E837–E844.

Lemaçon, D., Jackson, J., Quinet, A., Brickner, J.R., Li, S., Yazinski, S., You, Z., Ira, G., Zou, L., Mosammaparast, N., and Vindigni, A. (2017). MRE11 and EXO1 nucleases degrade reversed forks and elicit MUS81-dependent fork rescue in BRCA2-deficient cells. Nat. Commun. *8*, 860.

Marra, G., Iaccarino, I., Lettieri, T., Roscilli, G., Delmastro, P., and Jiricny, J. (1998). Mismatch repair deficiency associated with overexpression of the *MSH3* gene. Proc. Natl. Acad. Sci. USA *95*, 8568–8573.

Marsischky, G.T., and Kolodner, R.D. (1999). Biochemical characterization of the interaction between the *Saccharomyces cerevisiae* MSH2-MSH6 complex and mispaired bases in DNA. J. Biol. Chem. *274*, 26668–26682.

Marsischky, G.T., Filosi, N., Kane, M.F., and Kolodner, R. (1996). Redundancy of *Saccharomyces cerevisiae* MSH3 and MSH6 in MSH2-dependent mismatch repair. Genes Dev. *10*, 407–420.

Marsischky, G.T., Lee, S., Griffith, J., and Kolodner, R.D. (1999). *Saccharomyces cerevisiae* MSH2/6 complex interacts with Holliday junctions and facilitates their cleavage by phage resolution enzymes. J. Biol. Chem. *274*, 7200–7206.

Martinez, A.R., Kaul, Z., Parvin, J.D., and Groden, J. (2017). Differential requirements for DNA repair proteins in immortalized cell lines using alternative lengthening of telomere mechanisms. Genes Chromosomes Cancer *56*, 617–631.

McPherson, J.P., Lemmers, B., Chahwan, R., Pamidi, A., Migon, E., Matysiak-Zablocki, E., Moynahan, M.E., Essers, J., Hanada, K., Poonepalli, A., et al. (2004). Involvement of mammalian Mus81 in genome integrity and tumor suppression. Science *304*, 1822–1826.

Muñoz, I.M., Hain, K., Déclais, A.C., Gardiner, M., Toh, G.W., Sanchez-Pulido, L., Heuckmann, J.M., Toth, R., Macartney, T., Eppink, B., et al. (2009). Coordination of structure-specific nucleases by human SLX4/BTBD12 is required for DNA repair. Mol. Cell *35*, 116–127.

Owen, B.A., Yang, Z., Lai, M., Gajec, M., Badger, J.D., 2nd, Hayes, J.J., Edelmann, W., Kucherlapati, R., Wilson, T.M., and McMurray, C.T. (2005). (CAG)(n)-hairpin DNA binds to Msh2-Msh3 and changes properties of mismatch recognition. Nat. Struct. Mol. Biol. *12*, 663–670.

Panier, S., Maric, M., Hewitt, G., Mason-Osann, E., Gali, H., Dai, A., Labadorf, A., Guervilly, J.H., Ruis, P., Segura-Bayona, S., et al. (2019). SLX4IP antagonizes promiscuous BLM activity during ALT maintenance. Mol. Cell *76*, 27–43.e11.

Panigrahi, G.B., Slean, M.M., Simard, J.P., Gileadi, O., and Pearson, C.E. (2010). Isolated short CTG/CAG DNA slip-outs are repaired efficiently by hMutSβ, but clustered slip-outs are poorly repaired. Proc. Natl. Acad. Sci. USA *107*, 12593–12598.

Park, J.M., Huang, S., Tougeron, D., and Sinicrope, F.A. (2013). MSH3 mismatch repair protein regulates sensitivity to cytotoxic drugs and a histone deacetylase inhibitor in human colon carcinoma cells. PLoS ONE *8*, e65369.

Pluciennik, A., Dzantiev, L., Iyer, R.R., Constantin, N., Kadyrov, F.A., and Modrich, P. (2010). PCNA function in the activation and strand direction of MutLα endonuclease in mismatch repair. Proc. Natl. Acad. Sci. USA *107*, 16066–16071.

Pluciennik, A., Burdett, V., Baitinger, C., Iyer, R.R., Shi, K., and Modrich, P. (2013). Extrahelical (CAG)/(CTG) triplet repeat elements support proliferating cell nuclear antigen loading and MutLα endonuclease activation. Proc. Natl. Acad. Sci. USA *110*, 12277–12282.

Prakash, R., Zhang, Y., Feng, W., and Jasin, M. (2015). Homologous recombination and human health: the roles of BRCA1, BRCA2, and associated proteins. Cold Spring Harb. Perspect. Biol. *7*, a016600.

Rass, U., and West, S.C. (2006). Synthetic junctions as tools to identify and characterise Holliday junction resolvases. Methods Enzymol. *408*, 485–501.

Rass, U., Compton, S.A., Matos, J., Singleton, M.R., Ip, S.C.Y., Blanco, M.G., Griffith, J.D., and West, S.C. (2010). Mechanism of Holliday junction resolution by the human GEN1 protein. Genes Dev. *24*, 1559–1569.

Rogacheva, M.V., Manhart, C.M., Chen, C., Guarne, A., Surtees, J., and Alani, E. (2014). Mlh1-Mlh3, a meiotic crossover and DNA mismatch repair factor, is a Msh2-Msh3-stimulated endonuclease. J. Biol. Chem. *289*, 5664–5673.

Sarbajna, S., Davies, D., and West, S.C. (2014). Roles of SLX1-SLX4, MUS81-EME1, and GEN1 in avoiding genome instability and mitotic catastrophe. Genes Dev. *28*, 1124–1136.

Sarkar, J., Wan, B., Yin, J., Vallabhaneni, H., Horvath, K., Kulikowicz, T., Bohr, V.A., Zhang, Y., Lei, M., and Liu, Y. (2015). SLX4 contributes to telomere preservation and regulated processing of telomeric joint molecule intermediates. Nucleic Acids Res. *43*, 5912–5923.

Savouret, C., Brisson, E., Essers, J., Kanaar, R., Pastink, A., te Riele, H., Junien, C., and Gourdon, G. (2003). CTG repeat instability and size variation timing in DNA repair-deficient mice. EMBO J. *22*, 2264–2273.

Shah Punatar, R., and West, S.C. (2018). Preparation and resolution of Holliday junction DNA recombination intermediates. Methods Enzymol. *600*, 569–590.

Singh, T.R., Ali, A.M., Busygina, V., Raynard, S., Fan, Q., Du, C.H., Andreassen, P.R., Sung, P., and Meetei, A.R. (2008). BLAP18/RMI2, a novel OB-fold-containing protein, is an essential component of the Bloom helicase-double Holliday junction dissolvasome. Genes Dev. *22*, 2856–2868.

Sobinoff, A.P., Allen, J.A., Neumann, A.A., Yang, S.F., Walsh, M.E., Henson, J.D., Reddel, R.R., and Pickett, H.A. (2017). BLM and SLX4 play opposing roles in recombination-dependent replication at human telomeres. EMBO J. *36*, 2907–2919.

Stoepker, C., Hain, K., Schuster, B., Hilhorst-Hofstee, Y., Rooimans, M.A., Steltenpool, J., Oostra, A.B., Eirich, K., Korthof, E.T., Nieuwint, A.W.M., et al. (2011). SLX4, a coordinator of structure-specific endonucleases, is mutated in a new Fanconi anemia subtype. Nat. Genet. *43*, 138–141.

Surtees, J.A., and Alani, E. (2006). Mismatch repair factor MSH2-MSH3 binds and alters the conformation of branched DNA structures predicted to form during genetic recombination. J. Mol. Biol. *360*, 523–536.

Svendsen, J.M., Smogorzewska, A., Sowa, M.E., O'Connell, B.C., Gygi, S.P., Elledge, S.J., and Harper, J.W. (2009). Mammalian BTBD12/SLX4 assembles a Holliday junction resolvase and is required for DNA repair. Cell *138*, 63–77.

Takahashi, M., Koi, M., Balaguer, F., Boland, C.R., and Goel, A. (2011). MSH3 mediates sensitization of colorectal cancer cells to cisplatin, oxaliplatin, and a poly(ADP-ribose) polymerase inhibitor. J. Biol. Chem. *286*, 12157–12165.

Takedachi, A., Despras, E., Scaglione, S., Guérois, R., Guervilly, J.H., Blin, M., Audebert, S., Camoin, L., Hasanova, Z., Schertzer, M., et al. (2020). SLX4 interacts with RTEL1 to prevent transcription-mediated DNA replication perturbations. Nat. Struct. Mol. Biol. *27*, 438–449.

Tian, L., Hou, C., Tian, K., Holcomb, N.C., Gu, L., and Li, G.M. (2009). Mismatch recognition protein MutSβ does not hijack (CAG)n hairpin repair in vitro. J. Biol. Chem. *284*, 20452–20456.

Van Criekinge, W., and Beyaert, R. (1999). Yeast two-hybrid: state of the art. Biol. Proced. Online *2*, 1–38.

van Oers, J.M., Edwards, Y., Chahwan, R., Zhang, W., Smith, C., Pechuan, X., Schaetzlein, S., Jin, B., Wang, Y., Bergman, A., et al. (2014). The MutSβ complex is a modulator of p53-driven tumorigenesis through its functions in both DNA double-strand break repair and mismatch repair. Oncogene *33*, 3939–3946.

Wan, B., Yin, J., Horvath, K., Sarkar, J., Chen, Y., Wu, J., Wan, K., Lu, J., Gu, P., Yu, E.Y., et al. (2013). SLX4 assembles a telomere maintenance toolkit by bridging multiple endonucleases with telomeres. Cell Rep. *4*, 861–869.

Warren, J.J., Pohlhaus, T.J., Changela, A., Iyer, R.R., Modrich, P.L., and Beese, L.S. (2007). Structure of the human MutSα DNA lesion recognition complex. Mol. Cell *26*, 579–592.

Wechsler, T., Newman, S., and West, S.C. (2011). Aberrant chromosome morphology in human cells defective for Holliday junction resolution. Nature *471*, 642–646.

Wilson, T., Guerrette, S., and Fishel, R. (1999). Dissociation of mismatch recognition and ATPase activity by hMSH2-hMSH3. J. Biol. Chem. *274*, 21659–21664.

Wilson, J.S., Tejera, A.M., Castor, D., Toth, R., Blasco, M.A., and Rouse, J. (2013). Localization-dependent and -independent roles of SLX4 in regulating telomeres. Cell Rep. *4*, 853–860.

Wu, L., and Hickson, I.D. (2003). The Bloom's syndrome helicase suppresses crossing over during homologous recombination. Nature *426*, 870–874.

Wu, L., Davies, S.L., Levitt, N.C., and Hickson, I.D. (2001). Potential role for the BLM helicase in recombinational repair via a conserved interaction with RAD51. J. Biol. Chem. *276*, 19375–19381.

Wu, L., Bachrati, C.Z., Ou, J., Xu, C., Yin, J., Chang, M., Wang, W., Li, L., Brown, G.W., and Hickson, I.D. (2006). BLAP75/RMI1 promotes the BLM-dependent dissolution of homologous recombination intermediates. Proc. Natl. Acad. Sci. USA *103*, 4068–4073.

Wu, W., Bhowmick, R., Vogel, I., Özer, Ö., Ghisays, F., Thakur, R.S., Sanchez de Leon, E., Richter, P.H., Ren, L., Petrini, J.H., et al. (2020). RTEL1 suppresses G-quadruplex-associated R-loops at difficult-to-replicate loci in the human genome. Nat. Struct. Mol. Biol. *27*, 424–437.

Wyatt, H.D.M., Sarbajna, S., Matos, J., and West, S.C. (2013). Coordinated actions of SLX1-SLX4 and MUS81-EME1 for Holliday junction resolution in human cells. Mol. Cell *52*, 234–247.

Wyatt, H.D.M., Laister, R.C., Martin, S.R., Arrowsmith, C.H., and West, S.C. (2017). The SMX DNA repair tri-nuclease. Mol. Cell *65*, 848–860.e11.

Zhang, H., Chen, Z., Ye, Y., Ye, Z., Cao, D., Xiong, Y., Srivastava, M., Feng, X., Tang, M., Wang, C., et al. (2019). SLX4IP acts with SLX4 and XPF-ERCC1 to promote interstrand crosslink repair. Nucleic Acids Res. *47*, 10181–10201.

# Cell Reports
## Article

# STAR★METHODS

## KEY RESOURCES TABLE

| REAGENT or RESOURCE | SOURCE | IDENTIFIER |
| --- | --- | --- |
| **Antibodies** | | |
| Mouse monoclonal anti alpha-tubulin | Sigma-Aldrich | Cat# 00020911; RRID: AB_10013740 |
| Mouse monoclonal anti-GFP | Roche | Cat# ABN421; RRID: AB_390913 |
| Mouse monoclonal anti-H3 phospho S10 | Abcam | Cat# ab14955; RRID: AB_443110 |
| Mouse monoclonal anti-MSH2 | Abcam | Cat# ab52266; RRID: AB_2144800 |
| Mouse monoclonal anti-MSH3 | BD Bioscience | Cat# 611390; RRID: AB_398912 |
| Mouse monoclonal anti-MSH6 | BD Bioscience | Cat# 610918; RRID: AB_398233 |
| Mouse monoclonal anti-MUS81 | Santa Cruz Biotechnology | Cat# sc-53382; RRID: AB_2147138 |
| Mouse monoclonal anti-XPF | Abcam | Cat# ab3299; RRID: AB_303684 |
| Rabbit monoclonal anti-GEN1 | Stephen West lab | Rass et al., 2010 |
| Sheep polyclonal anti-SLX1 | John Rouse lab | Muñoz et al., 2009 |
| Sheep polyclonal anti-SLX4 | John Rouse lab | Muñoz et al., 2009 |
| Mouse monoclonal anti-Cyclin A | Santa Cruz Biotechnology | Cat# sc-56299; RRID: AB_782328 |
| Mouse monoclonal anti-RPA2 | Abcam | Cat# ab2175; RRID: AB_302873 |
| Rabbit polyclonal anti-FANCD2 | Novus Biologicals | Cat# NB100-182; RRID: AB_10002867 |
| Rabbit polyclonal anti-MDC1 | Abcam | Cat# ab11169; RRID: AB_297807 |
| Goat anti-mouse Immunoglobulins/HRP | Agilent | Cat# P0447; RRID: AB_2617137 |
| Goat anti-rabbit Immunoglobulins/HRP | Agilent | Cat# P0448; RRID: AB_2617138 |
| Rabbit anti-sheep Immunoglobulins/HRP | Abcam | Cat# ab6747 |
| Alexa Fluor 488 Goat anti-Mouse IgG (H+L) | ThermoFisher | Cat# A-32723 RRID: AB_2633275 |
| Alexa Fluor 488 Goat anti-Rabbit IgG (H+L) | ThermoFisher | Cat# A-11070; RRID: AB_2534114 |
| Alexa Fluor 546 Donkey anti-Mouse IgG (H+L) | ThermoFisher | Cat# A-10036; RRID: AB_2534012 |
| Alexa Fluor 546 Donkey anti-Rabbit IgG (H+L) | ThermoFisher | Cat# A-10040; RRID: AB_2534016 |
| **Bacterial and Virus Strains** | | |
| *Escherichia coli*: Max efficiency DH10Bac Competent cells | ThermoFisher | Cat# 10361012 |
| *Escherichia coli*: MultiBac competent cells | Imre Berger lab | Fitzgerald et al., 2006 |
| *Escherichia coli*: One Shot TOP10 Competent Cells | ThermoFisher | Cat# 4040-06 |
| **Chemicals, Peptides, and Recombinant Proteins** | | |
| [$\gamma$-$^{32}$P]-ATP (3000 Ci/mmol, 10 mCi/mL, EasyTide Lead) | PerkinElmer | Cat# NEG502A100UC |
| Acetic acid | ThermoFisher | Cat#10304980 |
| Acrylamide/Bis 37.5:1 (30%) | Biorad | Cat# 1610158 |
| Acrylamide/Bis-acrylamide 19:1 (40%) | Biorad | Cat# 1610144 |
| Ampicillin sodium salt | Sigma-Aldrich | Cat# A0166 |
| Bradford Assay | ThermoFisher | Cat# 23236 |
| BrdU | Sigma-Aldrich | Cat# 19-160 |
| Cisplatin | Sigma-Aldrich | Cat# 15663-27-1 |
| Colcemid | Roche | Cat# 10295892001 |
| cOmplete, Mini, EDTA-free Protease Inhibitor Cocktail | Roche | Cat# 11836170001 |
| CTP, [$\alpha$-$^{32}$P]-CTP (3000Ci/mmol 10mCi/ml, 250 μCi) | PerkinElmer | Cat# BLU008H250UC |

*(Continued on next page)*

*Continued*

| REAGENT or RESOURCE | SOURCE | IDENTIFIER |
|---|---|---|
| D-Biotin | Sigma-Aldrich | Cat# B4501 |
| DC Protein Assay | Bio-Rad | Cat# 5000111 |
| DO Supplement -Leu/-Trp | Takara | Cat# 630417 |
| DO Supplement -Leu/-Trp/-His | Takara | Cat# 6304419 |
| Ethanol | Sigma-Aldrich | Cat# E7023 |
| Gentamicin sulfate salt | Sigma-Aldrich | Cat# G1264 |
| Giemsa | Sigma-Aldrich | Cat# G5637 |
| Hoechst 33342 | Sigma-Aldrich | Cat# B2261 |
| Imidazole | Sigma | Cat#I5513 |
| InstantBlue Stain | Gentaur | Cat# ISB1L |
| IPTG | Roche | Cat# IPTG-RO |
| Isopropanol | Sigma-Aldrich | Cat# I9516 |
| Kanamycin Monosulphate | Formedium | Cat# KAN0025 |
| Methanol | ThermoFisher | Cat# 10396090 |
| Nocodazole | Sigma-Aldrich | Cat# 31430-18-9 |
| PhosSTOP phosphatase inhibitors | Roche | Cat# 04906845001 |
| Pierce 16% Formaldehyde, Methanol-free | ThermoFisher | Cat# 28906 |
| Platinum Quantitative PCR SuperMix-UDG | ThermoFisher | Cat# 11730025 |
| Proteinase K | Sigma-Aldrich | Cat# P4850 |
| Restriction Enzymes | NEB | https://www.neb.uk.com/ |
| SYPRO Ruby Stain | ThermoFisher | Cat# S12000 |
| T4 Polynucleotide Kinase | NEB | Cat# M0201S |
| Tetracycline | Sigma-Aldrich | Cat# 87128 |
| Thymidine | Sigma-Aldrich | Cat# T1895 |
| X-Gal | Roche | Cat# XGAL-RO |
| Peptide: 3x FLAG | The Francis Crick Institute Peptide Chemistry Scientific Technology Platform | N/A |
| Recombinant Protein: Human MSH2-$_{HIS6}$MSH3 (MutSβ) | This paper | N/A |
| Recombinant Protein: Human MSH2-$_{HIS6}$MSH6 (MutSα) | This paper | N/A |
| Recombinant Protein: Human $_{V5}$SLX1-$_{STREP}$SLX4 | This paper | N/A |
| Recombinant Protein: Human $_{STREP}$SLX4 | This paper | N/A |
| Recombinant Protein: Human SMX ($_{V5}$SLX1-$_{STREP}$SLX4-MUS81-$_{FLAG}$EME1-$_{HIS6}$XPF-ERCC1) | This paper | N/A |
| Recombinant Protein: Human SLX1-SLX4$^{CCD}$ (SLX1-$_{HIS10}$SLX4$^{1664-1834}$$_{STREP}$) | This paper | N/A |
| Critical Commercial Assays | | |
| baculoQuant One-Step Titration kit | Oxford Expression Technologies | Cat# 10060 |
| Frozen-EZ Yeast II transformation kit | Zymo Research | Cat# T2001 |
| FuGENE HD transfection reagent | Promega | Cat#: E2311 |
| Gateway LR Clonase II enzyme mix | ThermoFisher | Cat#: 11791020 |
| GFP-Trap MA resin | Chromtek | Cat#: gtma-10 |
| Gibson Assembly cloning kit | NEB | Cat#: E5510S |
| HiTRAP Q HP column, 1 mL | GE Healthcare | Cat# 17-1153-01 |
| Lipofectamine RNAi MAX reagent | ThermoFisher | Cat#: 13778075 |
| Microspin G-25 spin column | Sigma-Aldrich | Cat# GE27-5325-01 |

*Continued*

| REAGENT or RESOURCE | SOURCE | IDENTIFIER |
|---|---|---|
| Ni-NTA agarose resin | ThermoFisher | Cat# R90101 |
| Pfu Ultra High-Fidelity DNA Polymerase | Agilent | Cat#: 600380 |
| Purelink HiPure plasmid DNA purification kit | ThermoFisher | Cat# K2100-02 |
| QIAprep Spin Miniprep Kit | QIAGEN | Cat# 27106 |
| Slide-A-Lyzer G2 dialysis cassette, 10 MWCO | Pierce | Cat# 87730 |
| Streptactin XT resin | IBA Lifesciences | Cat# 2-4010-002 |
| Experimental Models: Cell Lines | | |
| Human: GM08505 SV40-transformed Bloom's syndrome fibroblasts | The Francis Crick Institute Cell Services | Wu et al., 2001 |
| Human: HEK293T | The Francis Crick Institute Cell Services | N/A |
| Human: HeLa-Kyoto | The Francis Crick Institute Cell Services | N/A |
| Human: T-REx-293 | The Francis Crick Institute Cell Services | N/A |
| Human: T-REx-293 $GEN1^{-/-}$ | Stephen West lab | Chan et al., 2018 |
| *S. frugiperda:* SF9 | The Francis Crick Institute Cell Services | N/A |
| Experimental Models: Organisms/Strains | | |
| *S. cerevisiae*: Strain background: L40 | ATCC | ATCC MYA3332 |
| Oligonucleotides | | |
| siRNA: ON-TARGETplus Non-targeting Control siRNA #1 | Dharmacon, Horizon Discovery | Cat# D-001810-01-05 |
| siRNA: MSH3 siRNA: #1: 5′-UCGAGUCGAAAGGAUGGAUAAdTdT-3′ | Sigma-Aldrich | Burdova et al., 2015 |
| siRNA: MSH3 siRNA: #2: 5′-CAGCAAGGAGUUAUGGAUUAAdTdT-3′ | Sigma-Aldrich | Burdova et al., 2015 |
| siRNA: MSH3 siRNA: #3: 5′-TGCAACCAGTTTATCCACCAAdTdT-3′ | Sigma-Aldrich | Burdova et al., 2015 |
| siRNA: MSH6 siRNA: #1: 5′-AUCGCCAUUGUUCGAGAUUUAdTdT-3′ | Sigma-Aldrich | Burdova et al., 2015 |
| siRNA: MSH6 siRNA: #2: 5′-CAGCAGGGCUAUAAUGUAUGAdTdT-3′ | Sigma-Aldrich | Burdova et al., 2015 |
| siRNA: SLX4 siRNA: 5-AAACGUGAAUGAAGCAGAAUU-3′ and 5-CGGCAUUUGAGUCUGCAGGUGAA-3′ | Sigma-Aldrich | Fekairi et al., 2009; Muñoz et al., 2009; Svendsen et al., 2009 |
| siRNA: SMARTpool ON-TARGETplus GEN1 siRNA #1 | Dharmacon, Horizon Discovery | Cat# L-018757-02-0005 |
| Primer: SLX1$^{R41A}$ forward: 5′-CCCTGGCGGTGTTGACGGTGAATCCG-3′ | Sigma-Aldrich | N/A |
| Primer: SLX1$^{R41A}$ reverse: 5′-CAGTCCAGCAGCACAACGGTGGACGC-3 | Sigma-Aldrich | N/A |
| Primer: SLX1$^{E82A}$ forward: 5′-GCGAAGCGCAGGGCGGCG-3′ | Sigma-Aldrich | N/A |
| Primer: SLX1$^{E82A}$ reverse: 5′-ATGGGCCTGGCAGCACCCTCAC-3′ | Sigma-Aldrich | N/A |
| Oligonucleotides for nuclease and DNA-binding experiments: see Table S2 | Sigma-Aldrich | N/A |
| Recombinant DNA | | |
| Plasmid: pCDNA3.1-GFP | Simon Boulton lab | Panier et al., 2019 |
| Plasmid: pCDNA3.1-GFP-SLX41-1834aa | Simon Boulton lab | Panier et al., 2019 |
| Plasmid: pCR8 GW/TOPO/TA | ThermoFisher | Cat# K250020 |
| Plasmid: pCR8-MSH2 | This paper | N/A |

*(Continued on next page)*

**Continued**

| REAGENT or RESOURCE | SOURCE | IDENTIFIER |
|---|---|---|
| Plasmid: pCR8-MSH3 | This paper | N/A |
| Plasmid: pCR8-MSH6 | This paper | N/A |
| Plasmid: pCR8-MUS81 | This paper | N/A |
| Plasmid: pCR8-GEN1 | This paper | N/A |
| Plasmid: pENTR6-SLX4 | This paper | N/A |
| Plasmid: pCR8-GFP | This paper | N/A |
| Plasmid: pLexA-GW | Addgene | Cat# 11345 |
| Plasmid: pLexA-MSH2 | This paper | N/A |
| Plasmid: pLexA-MSH3 | This paper | N/A |
| Plasmid: pLexA-MSH6 | This paper | N/A |
| Plasmid: pLexA-MUS81 | This paper | N/A |
| Plasmid: pLexA-GEN1 | This paper | N/A |
| Plasmid: pLexA-GFP | This paper | N/A |
| Plasmid: pGADT7-GW | Addgene | Cat# 61702 |
| Plasmid: pGADT7-SLX4 | This paper | N/A |
| Plasmid: pGADT7-GFP | This paper | N/A |
| Plasmid: pFastBAC1-$_{HIS6}$MSH6 | Cynthia McMurray lab | Unpublished |
| Plasmid: pDest8 | ThermoFisher | Cat# 11804010 |
| Plasmid: pDest8-MSH2 | This paper | N/A |
| Plasmid: pFastBAC-Dual MSH2-$_{HIS6}$MSH3 | Cynthia McMurray lab | Owen et al., 2005 |
| Plasmid: pFastBAC-Dual-$_{V5}$SLX1-$_{STREP}$SLX4 | This paper | N/A |
| Plasmid: pFastBAC-Dual-$_{HIS6}$XPF-ERCC1 | This paper | N/A |
| Plasmid: pFL-MUS81-$_{FLAG}$EME1 | Stephen West lab | Wyatt et al., 2013 |
| Plasmid:pFastBAC-Dual-$_{V5}$SLX1$^{R41A/E82A}$$_{STREP}$SLX4 | This paper | N/A |
| Plasmid: pBIG1a | Addgene | Cat# 80611 |
| Plasmid: pBIG1a-SLX1-$_{HIS10}$SLX4$^{1664-1834aa}$$_{STREP}$ | This paper | N/A |
| Plasmid: pDEA-7Z | Stephen West lab | Shah Punatar and West, 2018 |
| Plasmid: pDEA2 | Stephen West lab | Shah Punatar and West, 2018 |
| Bacmid: MSH2 | This paper | N/A |
| Bacmid: $_{HIS6}$MSH6 | This paper | N/A |
| Bacmid: MSH2-$_{HIS6}$MSH3 | This paper | N/A |
| Bacmid: $_{V5}$SLX1$^{R41A/E82A}$-$_{STREP}$SLX4 | This paper | N/A |
| Bacmid: $_{V5}$SLX1-$_{STREP}$SLX4 | This paper | N/A |
| Bacmid: MUS81-$_{FLAG}$EME1 | This paper | N/A |
| Bacmid: $_{HIS6}$XPF-ERCC1 | This paper | N/A |
| Bacmid: SLX1-$_{HIS10}$SLX4$^{1664-1834}$$_{STREP}$ | This paper | N/A |
| Software and Algorithms | | |
| BLI Acquisition and analysis software 9.0 | FortéBio | https://www.fortebio.com/products/octet-systems-software |
| Graphpad Prism 8 for Mac OS X | GraphPad Software | https://www.graphpad.com/scientific-software/prism/ |
| ImageQuant TL v2005 | GE Healthcare | https://imagequant-tl-v2005.software.informer.com/ |
| Volocity v6.3 software | Perkin Elmer | https://www.perkinelmer.com/uk/lab-solutions/resources/docs/BRO_VolocityBrochure_PerkinElmer.pdf |

*Continued*

| REAGENT or RESOURCE | SOURCE | IDENTIFIER |
|---|---|---|
| Other | | |
| Amersham Protran 0.2 NC 300mm x 4 m | Sigma-Aldrich | Cat# GE10600001 |
| BioCoat Poly-D-Lysine glass coverslip 12mm | Corning | Cat# 354087 |
| DPX mountant for histology | Sigma-Aldrich | Cat# 06522 |
| Fetal Bovine Serum | Sigma-Aldrich | Cat# F2442 |
| GIBCO DMEM medium | ThermoFisher | Cat# 11995073 |
| GIBCO Opti-MEM Medium | ThermoFisher | Cat# 31985062 |
| GIBCO SF900-III SFM Medium | ThermoFisher | Cat# 12658027 |
| Hard-Shell Thin-Wall 96-Well Skirted PCR Plates | Bio-Rad | Cat# HSP-9655 |
| Invitrogen NuPAGE 4-12% Bis-Tris Protein Gels | ThermoFisher | Cat# NP0321BOX |
| Microseal 'B' Adhesive Seals | Bio-Rad | Cat# MSB-1001 |
| ProLong Gold Antifade Mountant with DAPI | ThermoFisher | Cat# P36935 |

## RESOURCE AVAILABILITY

### Lead Contact
Further information and requests for resources should be directed to and will be fulfilled by the Lead Contact, Stephen C. West (stephen.west@crick.ac.uk).

### Materials Availability
All unique/stable reagents generated in this study are available from the Lead Contact without restriction.

### Data and Code Availability
The published article contains all datasets generated or analyzed during this study.

## EXPERIMENTAL MODEL AND SUBJECT DETAILS

HeLa-Kyoto cells (HelaK), T-REx-293 wild-type and T-REx-293 $GEN1^{-/-}$ cells (Chan et al., 2018) were cultured in GIBCO DMEM supplemented with 10% FBS (Sigma Aldrich). GM08505 cells were cultured in GIBCO DMEM supplemented with 20% FBS (Sigma Aldrich). All cells were maintained in a humidified environment at 37°C with 5% $CO_2$.

## METHOD DETAILS

### Plasmids
pCR8 entry vectors pCR8-MSH2, pCR8-MSH3, pCR8-MSH6, pCR8-MUS81, pCR8-GEN1, pENTR6-SLX4 and pCR8-GFP were generated by Gateway® recombination between pCR8 vector (Addgene) and a PCR fragment containing the desired gene. One Shot TOP10 competent *E. coli* cells (ThermoFisher) were transformed and selected on LB plates containing 50 μg/ml spectinomycin. PCRs were conducted using Phusion High-Fidelity Polymerase (ThermoFisher). The PCR primers used to generate the pCR8 entry vectors were:

MSH2:
5′-gcggtgcagccgaa-3′ and 5′-tcacgtagtaactttattcgtgaaatg-3′
MSH3:
5′-tctcgccggaagcct-3′ and 5′-ttaatgaagaagagaagtctgtgtttct-3′
MSH6:
5′-tcgcgacagagcaccc-3′ and
5′-ctataattccttaatcaaagtcagcaatttatg-3′
MUS81:
5′-atggcggccccggt-3′ and 5′-tcaggtcaaggggccgt-3′
GEN1:

5′-ggagtgaatgacttgtggcaaattt-3′ and
5′-tcaagtgctttggaatcttagtttttaatctc-3′
SLX4:
5′-aaactgagtgtgaatgaggctc-3′ and 5′-tcagttccgctccacctt-3′
GFP:
5′-GTGAGCAAGGGCGAGGA-3′ and 5′-CTTGTACAGCTCGTCCATGCC-3′

Destination vectors pLexA-MSH2, pLexA-MSH3, pLexA-MSH6, pLexA-MUS81, pLexA-GEN1, pLexA-GFP, pGADT7-SLX4 and pGADT7-GFP were cloned from the appropriate pCR8 entry vector by recombination with pLexA or pGADT7 (Addgene) using Gateway® LR Clonase II enzyme mix (ThermoFisher). pCDNA3.1-GFP and pCDNA3.1-SLX4$_{GFP}$ were a generous gift from Dr Simon Boulton (Panier et al., 2019). pFastBAC Dual-MSH2-$_{HIS6}$MSH3, pFastBAC1-$_{HIS6}$MSH2 and pFastBAC1-$_{HIS6}$MSH6 were a kind gift from Dr Cynthia McMurray (Owen et al., 2005). pDest8-MSH2 was generated by recombination between pDest8 (ThermoFisher) and pCR8-MSH2 using Gateway® L4 Clonase II enzyme mix (ThermoFisher). One Shot Top10 competent *E. coli* cells (ThermoFisher) were transformed and selected on LB plates containing 75 μg/ml ampicillin. pFastBAC Dual-$_{V5}$SLX1-$_{STREP}$SLX4 was generated by PCR amplifying $_{V5}$SLX1 and $_{STREP}$SLX4, codon optimized for expression in Hi5 insect cells (Wyatt et al., 2017), and cloning into the SalI/HindIII and XhoI/NheI sites of pFastBac Dual, respectively. pFastBAC Dual-$_{HIS6}$XPF-ERCC1 was generated by amplifying $_{HIS6}$XPF and ERCC1 and cloning into the NheI/SphI and SalI/NotI sites of pFastBAC Dual. For all pFastBAC Dual constructs, PCRs were conducted using PfuUltra High-Fidelity DNA Polymerase (Agilent), and restriction and ligation reactions were carried out using enzymes from New England Biolabs.

pFastBAC Dual-$_{V5}$SLX1$^{R41A/E82A}$-$_{STREP}$SLX4 was generated from pFastBAC Dual-$_{V5}$SLX1-$_{STREP}$SLX4 by sequential PCR of the entire plasmid using primers that introduce the relevant mutations (SLX1$^{R41A}$: 5′-CCCTGGCGGTGTTGACGGTGAATCCG-3′ and 5′-CAGTCCAGCAGCACAACGGTGGACGC-3′, and SLX1$^{E82A}$: 5′-GCGAAGCGCAGGGCGGCG-3′ and 5′-ATGGGCCTGGCAG-CACCCTCAC-3′). pFL-MUS81-$_{FLAG}$EME1 is described elsewhere (Wyatt et al., 2013).

pBig1a-SLX1-$_{HIS10}$SLX4$^{1664-1834aa}$$_{STREP}$ (SLX1-SLX4$^{CCD}$) was cloned using Gibson Assembly (NEB). Gene blocks comprising the cDNA sequence for full length human SLX1 (codon optimized for expression in SF9 cells), and human $_{HIS10}$SLX4$^{1664-1834aa}$$_{STREP}$ flanked by alpha and omega cloning sites, respectively, were generated (Integrated DNA Technologies).

### siRNA

The following siRNAs were used.
control siRNA:
ON-TARGET plus D-001810-01-05 (Dharmacon, Horizon Discovery)
MSH3 siRNA:

#1: 5′-UCGAGUCGAAAGGAUGGAUAAdTdT-3′,
#2: 5′-CAGCAAGGAGUUAUGGAUUAAdTdT-3′
#3: 5′-TGCAACCAGTTTATCCACCAAdTdT-3′ (Burdova et al., 2015)

MSH6 siRNA:

#1: 5′-AUCGCCAUUGUUCGAGAUUUAdTdT-3′
#2: 5′-CAGCAGGGCUAUAAUGUAUGAdTdT-3′ (Burdova et al., 2015)

SLX4 siRNA:

#1: 5′- AAACGUGAAUGAAGCAGAAUU-3′
#2: 5′- CGGCAUUUGAGUCUGCAGGUGAA-3′ (Fekairi et al., 2009; Muñoz et al., 2009; Svendsen et al., 2009)

GEN1 siRNA:

SMARTpool ON-TARGETplus L-018757-02-0005 (Dharmacon, Horizon Discovery)

### Antibodies

Proteins were detected by western blotting using the following antibodies: mouse anti-MSH2 (ABCAM ab52266), mouse anti-MSH3 (BD Bioscience 611390), mouse anti-MSH6 (BD Bioscience 610918), mouse anti-MUS81 (Santa Cruz MTA30 2G/10 sc-53382), mouse anti-XPF (ABCAM ab3299), mouse anti-GFP (Roche 11814460001), mouse anti-pH3 (S10) (ABCAM ab14955), mouse anti-α-tubulin (Sigma Aldrich 00020911), rabbit anti-GEN1 (Rass et al., 2010) SLX1 and SLX4 were detected using sheep polyclonal antibodies (a kind gift from Professor John Rouse, Dundee University) (Muñoz et al., 2009). All primary antibodies were used at a 1:1000 dilution. Goat anti-mouse P0477 (DAKO Agilent), Goat anti-rabbit P0477 (DAKO Agilent), and rabbit anti-sheep (ABCAM ab6747) HRP-conjugated secondary antibodies were used at a 1:5000 dilution. For immunofluorescence analyses, the primary antibodies were mouse anti-RPA2 (ABCAM ab2175, dilution 1:1000), rabbit anti-FANCD2 (Novus NB100-182, dilution 1:1000), rabbit anti-

MDC1 (Abcam ab11169, dilution 1:1000), mouse anti-cyclin A (Santa Cruz Biotechnology sc-56299, dilution 1:200). Secondary antibodies were conjugated to Alexa Fluor 488 and Alexa Fluor 546 (ThermoFisher, dilution 1:2000). DNA was stained with DAPI using Prolong Diamond antifade mountant (ThermoFisher).

### Human cell culture and transfection

HeLa-Kyoto cells (HelaK), T-REx-293 wild-type and T-REx-293 $GEN1^{-/-}$ cells (Chan et al., 2018) were cultured in GIBCO DMEM supplemented with 10% FBS (Sigma Aldrich). GM08505 cells were cultured in GIBCO DMEM supplemented with 20% FBS (Sigma Aldrich). All cells were maintained in a humidified environment at 37°C with 5% $CO_2$.

To study interactions between SLX4 and MutSβ, pCDNA3.1-GFP or pCDNA3.1-SLX4$_{GFP}$ were transiently transfected into HEK293T cells. The cells were plated on Corning 150 × 25 mm dishes (ThermoFisher) and 25 μg of plasmid DNA was transfected using FuGENE HD transfection reagent (Promega). Cells were harvested for immunoprecipitation 24-48 hours after transfection.

### Ultrafine bridge formation and MDC1 immunofluorescence

To analyze ultra-fine anaphase bridge formation and MDC1 foci in G1, human T-REx-293 wild-type and $GEN1^{-/-}$ cells were plated onto Corning 6 well dishes (ThermoFisher) and siRNA depleted for the indicated proteins using Lipofectamine RNAi MAX reagent (ThermoFisher). 24 hours after siRNA transfection, cells were trypsinized and moved to sterile glass coverslips. For 53BP1 nuclear body analysis, cells were treated with cisplatin (1 μM) for 1 hour, followed by 24 hours recovery. Cells were harvested for fixation and immunofluorescence 48 hours after siRNA transfection.

### Sister chromatid exchanges

To analyze sister chromatid exchanges (SCEs), GM08505 cells were plated onto Corning 6 well dishes (ThermoFisher) and siRNA depleted for the indicated proteins using Lipofectamine RNAi MAX reagent (ThermoFisher). 24 hours after siRNA transfection, BrdU (100μM) was added, and cells were harvested 48 hours later. Metaphase spreads were fixed and stained as described (Wechsler et al., 2011).

### Cell synchronization

To study the temporal regulation of protein-protein interactions, HeLaK cells were transiently transfected with pCDNA3.1-GFP or pCDNA3.1-SLX4$_{GFP}$. Subsequently, cells were blocked in either G1/S or mitosis by treatment with thymidine (2 mM) (18-hour treatment, 8-hour release, followed by a second 16-hour treatment) or nocodazole (150 ng/ml) (16 hours), respectively. 48 hours after transfection the cells were harvested for lysis and immunoprecipitation.

### Cell lysis

Cells were collected by trypsinization, washed with PBS and resuspended in lysis buffer (25 mM HEPES pH 8.0, 150 mM NaCl, 1% Triton-X, 10% glycerol, 1 mM DTT) supplemented with cOmplete EDTA-free protease inhibitor cocktail (Sigma), and phosSTOP phosphatase inhibitors (Roche). Cells were passed through a 0.8 × 40 mm needle 5x and the soluble lysate was collected by centrifugation. To reduce the Triton-X concentration, lysates were diluted 5x in dilution buffer (25 mM HEPES pH 8.0, 150 mM NaCl, 10% glycerol, 1 mM DTT).

### Immunoprecipitation and western blotting

For immunoprecipitation using whole cell extracts, 6 mg of extract was pre-incubated with 15 μL Protein A agarose beads (Sigma) for 60 min, with rotation at 4°C to remove non-specific interactions. Unbound lysate was incubated with GFP-Trap MA beads (Chromotek) for 60 min, with rotation at 4°C. Beads were rinsed with wash buffer (25 mM HEPES pH 8.0, 150 mM NaCl, 0.2% Triton-X, 10% glycerol, 1 mM DTT) for 3 × 5 min, with rotation at 4°C, and bound proteins were eluted by boiling the beads in 50 μL Laemmli sample buffer (BioRad) supplemented with DTT for 5 min at 95°C.

For immunoprecipitation of purified proteins, 1 μg of purified $_{V5}$SLX1-$_{STREP}$SLX4, SMX ($_{V5}$SLX1-$_{STREP}$SLX4–MUS81-$_{FLAG}$EME1-$_{HIS6}$XPF-ERCC1) or SLX1-SLX4$^{CCD}$ (SLX1-$_{HIS10}$SLX4$^{1664-1834}$$_{STREP}$) was incubated with 10 μg of purified MSH2-$_{HIS6}$MSH3 in immunoprecipitation buffer (25 mM HEPES pH 8.0, 150 mM NaCl, 2 mM MgCl$_2$ 1 mM ATP, 10% glycerol, 0.05% NP40, 1 mM DTT) for 10 min at 4°C. Reactions were then incubated with 5 μL of pre-equilibrated Streptactin XT beads (IBA Lifesciences) for 1 hour at 4°C with gentle agitation. Beads were washed with 3 × 1 mL immunoprecipitation buffer. Bound proteins were eluted by boiling the beads in 50 μL Laemmli sample buffer (Biorad) supplemented with DTT.

Proteins were separated on Novex NuPAGE 4%–12% Bis-Tris gels (ThermoFisher) and transferred to 0.2 μm nitrocellulose membranes in transfer buffer (25 mM Tris, 190 mM glycine, 20% methanol, 0.1% SDS) at 0.4 A for 60 min at 4°C. Proteins were detected by western blotting.

### Yeast two-hybrid analysis

Two hybrid assays were carried out essentially as described (Van Criekinge and Beyaert, 1999). In brief, L40 yeast cells were transformed with 0.5 μg of each of the indicated pLexA and pGADT7 vectors (1 μg total DNA), using Frozen-EZ Yeast II transformation kit (Zymo Research). Transformants were a grown on minimal media agar plates SC -TRP, -LEU for 48-72 hours at 30°C. To assay for

interactions, colonies were amplified in minimal media SC -TRP, -LEU for 16 hours at 30°C and 50000 cells were spotted on agar plates containing SC -TRP-LEU, SC -TRP -LEU -HIS and SC -TRP -LEU -HIS +160 µg/ml X-Gal (Sigma Aldrich). Plates were incubated for 48-96 hours at 30°C.

### Bacmid generation

To generate recombinant bacmids, plasmid DNA was transformed into Max Efficiency DH10Bac competent cells (ThermoFisher). For pFL-MUS81-EME1, bacteria was plated on LB agar plates containing 50 µg/ml kanamycin, 7 µg/ml gentamicin, 10 µg/ml tetracycline, 50 µg/ml spectinomycin, 400 µg/ml X-gal and 0.25 mM IPTG. For pFastBACDual-MSH2-$_{HIS6}$MSH3, pDest8-MSH2, pFastBAC1-$_{HIS6}$MSH6, pFastBACDual-$_{V5}$SLX1-$_{STREP}$SLX4, pFastBACDual-$_{HIS6}$XPF-ERCC1, pFastBACDual-$_{V5}$SLX1$^{R41A/E82A}$-$_{STREP}$SLX4 and pbiGBac-SLX1-$_{HIS10}$SLX4$^{1664-1834}$$_{STREP,}$ bacteria were plated onto LB agar plates containing 50 µg/ml kanamycin, 7 µg/ml gentamicin, 10 µg/ml tetracycline, 400 µg/ml X-gal and 0.25 mM IPTG and incubated at 37°C for 1-2 days until blue/white colonies were visible. White colonies were restreaked to verify successful transposition. True white colonies were inoculated into 2x YT medium and incubated at 37°C for 16 hours. Bacmid DNA was then purified using Purelink HiPure DNA Purification Kit (ThermoFisher) according to the manufacturer's guidelines.

### Baculovirus amplification

SF9 cells were cultured in GIBCO® Sf-900 III serum-free medium (ThermoFisher) and maintained in suspension at 28°C. P1 baculovirus was generated by transfecting 1 µg of bacmid DNA into 1 × 10$^6$ SF9 cells, using FuGENE transfection reagent, according to the manufacturer's guidelines. P1 virus was harvested at 66-72 hours post-transfection and viral DNA isolated using the High Pure Viral Nucleic Acid Kit (Roche). Viral titer was determined by qPCR using Platinum qPCR Supermix UDG (ThermoFisher) and the BaculoQUANT kit (Oxford Expression Technologies). P2 baculovirus were generated by infecting 2 × 10$^6$ cells/ml at a multiplicity of infection (MOI) of 0.01 and harvesting the media at 66-72 hours post-infection. Expression of recombinant protein was monitored by western blotting. For protein purification, 0.5 L to 1 L cultures at 2 × 10$^6$ cells/ml were infected with the relevant P2 baculovirus at a MOI of 1-5.

### Protein purification

MSH2-$_{HIS6}$MSH3 (MutSβ) and MSH2-$_{HIS6}$MSH6 (MutSα) were purified from approximately 3 × 10$^9$ SF9 cells infected with P2 baculovirus containing either MSH2-$_{HIS6}$MSH3 or MSH2-$_{HIS6}$MSH6 for 66 hours. Cells were resuspended in HNG300 (25 mM HEPES pH 8.0, 300 mM NaCl, 10% glycerol, 0.05% NP40, 1 mM DTT) supplemented with protease inhibitors (cOmplete EDTA-free tablets, Roche) and phosphatase inhibitors (PhosSTOP, Roche). The lysate was homogenized using a Dounce (20 strokes on ice), and chromatin sheared by sonication at 50% maximum amplitude for 4x 30 s. Soluble proteins were isolated by ultracentrifugation (Beckman Type JLA25.50 rotor) at 40000xg for 40 min at 4°C. The soluble extract was supplemented with 20 mM imidazole and incubated with 1 mL Ni-NTA beads (ThermoFisher Scientific) for 1 hour at 4°C. Beads were washed with HNG300 supplemented with 20 mM imidazole, and protein eluted with HNG300 buffer supplemented with 200 mM imidazole. Eluates were pooled, diluted to 100 mM NaCl using HG buffer (25 mM HEPES pH 8.0, 10% glycerol, 0.05% NP40 1 mM DTT) and loaded on to a pre-equilibrated 1ml HiTRAP Q HP column (GE Healthcare). Proteins were eluted with a linear gradient of 100 mM to 1 M NaCl and peak fractions identified by SDS-PAGE and Instant Blue (Gentaur) staining. Peak fractions were diluted to 150 mM NaCl using HG buffer and frozen in liquid nitrogen. For BLI, peak fractions were frozen undiluted. The MutSβ and MutSα concentrations were 1.5 µM and 2.5 µM respectively (assuming a 1:1 stoichiometry).

$_{V5}$SLX1-$_{STREP}$SLX4 was purified from approximately 3 × 10$^9$ SF9 cells infected with P2 baculovirus containing $_{V5}$SLX1-$_{STREP}$SLX4 for 66 hours. Cells were resuspended in pre-extraction buffer (25 mM HEPES pH 8.0, 10% glycerol, 1 mM DTT) supplemented with protease inhibitors (cOmplete EDTA-free tablets, Roche) and phosphatase inhibitors (PhosSTOP, Roche), incubated for 10 min on ice and homogenized by Dounce (20 strokes on ice) followed by centrifugation at 4000 rpm for 15 min at 4°C. The nuclear pellet was resuspended in HNG300 supplemented with protease and phosphatase inhibitors. Chromatin was sheared by sonication at 50% maximum amplitude for 4 × 30 s. Soluble proteins were isolated by ultracentrifugation (Beckman Type JLA25.50 rotor) at 40000xg for 40 min at 4°C. Soluble extracts were incubated with 2 mL Streptactin XT beads (IBA Lifesciences) for 1 hour at 4°C. Beads were washed in HNG300 buffer and protein eluted in HNG300 supplemented with 10 mM biotin. Eluates were pooled, diluted to 150 mM NaCl in HG and loaded on to a pre-equilibrated 1ml HiTRAP Q HP column (GE Healthcare). Protein was eluted with a linear gradient of 0.1 to 1 M NaCl and peak fractions identified by SDS-PAGE and Instant Blue (Gentaur) staining. Peak fractions were loaded into a Slide-A-Lyzer mini (Pierce) and dialyzed against 2 L storage buffer (50 mM Tris-HCl, pH 8.0, 100 mM NaCl, 10% glycerol, 1 mM EDTA, 1 mM DTT) and frozen in liquid nitrogen. The SLX1-SLX4 concentration was determined to be 920 nM (assuming a 1:1 stoichiometry).

$_{STREP}$SLX4 was purified from approximately 3 × 10$^9$ SF9 cells infected with P2 baculovirus containing $_{V5}$SLX1$^{R41A/E82A}$-$_{STREP}$SLX4 for 48 hours. Purification was conducted as described for $_{V5}$SLX1-$_{STREP}$SLX4. SLX1$^{R41A/E82A}$ was lost during the purification as verified by immunoblotting. The SLX4 concentration was determined to be 41 nM.

SMX ($_{V5}$SLX1-$_{STREP}$SLX4-MUS81-$_{FLAG}$EME1-$_{HIS6}$XPF-ERCC1) was purified from approximately 3 × 10$^9$ SF9 cells co-infected with P2 baculovirus containing $_{V5}$SLX1-$_{STREP}$SLX4, MUS81-$_{FLAG}$EME1 and $_{6xHIS}$XPF-ERCC1 for 66 hours. Cells were resuspended in pre-extraction buffer supplemented with protease inhibitors (cOmplete EDTA-free tablets, Roche) and phosphatase inhibitors

(PhosSTOP, Roche), incubated for 10 min on ice and homogenized using a Dounce (20 strokes on ice) followed by centrifugation at 4000 rpm for 15 min at 4°C. The nuclear pellet was resuspended in HNG500 (25 mM HEPES pH 8.0, 500 mM NaCl, 10% glycerol, 0.05% NP40, 1 mM DTT) supplemented with protease and phosphatase inhibitors. Chromatin was sheared by sonication at 50% maximum amplitude for 4 × 30 s. Soluble proteins were isolated by ultracentrifugation (Beckman Type JLA25.50 rotor) at 40000xg for 40 min at 4°C. The soluble extract was incubated with 2 mL FLAG-M2 beads (Sigma Aldrich) for 1 hour at 4°C. During the wash steps, the NaCl concentration was lowered stepwise from 500 mM to 300 mM, in 50 mM increments (in HG buffer). Proteins were eluted with 0.5 mg/ml 3x FLAG peptide in HNG300 buffer. Eluates were pooled, supplemented with 30 mM imidazole and incubated with 1 mL Ni-NTA beads (ThermoFisher Scientific) for 1 hour at 4°C. During the wash steps, the NaCl concentration was lowered stepwise from 300 mM to 200 mM, in 50 mM increments (in HG buffer). Proteins were eluted with HNG200 (25 mM HEPES pH 8.0, 200 mM NaCl, 10% glycerol, 0.05% NP40, 1 mM DTT) supplemented with 200 mM imidazole, pooled, supplemented with 1 mM EDTA and loaded on to a pre-equilibrated 1 mL HiTRAP Q HP column (GE Healthcare). Proteins were eluted with a linear gradient of 0.1 to 1 M NaCl in and peak fractions identified by SDS-PAGE and Instant Blue (Gentaur) staining. Peak fractions were loaded into a Slide-A-Lyzer mini (ThermoFisher), dialyzed against 2 L storage buffer and frozen in liquid nitrogen. The SMX concentration was determined to be 504 nM (assuming a 1:1:1:1:1 stoichiometry).

SLX1-SLX4$^{CCD}$ (SLX1-$_{HIS10}$SLX4$^{1664-1834}_{STREP}$) was purified from approximately $3 \times 10^9$ SF9 cells infected with P2 baculovirus containing SLX1-$_{HIS10}$SLX4$^{1664-1834}_{STREP}$ for 66 hours. Cells were resuspended in HNG300 supplemented with protease inhibitors (cOmplete EDTA-free tablets, Roche) and phosphatase inhibitors (PhosSTOP, Roche) and homogenized by Dounce (20 strokes on ice). Chromatin was sheared by sonication at 50% maximum amplitude for 4 × 30 s. Soluble proteins were isolated by ultracentrifugation (Beckman Type JLA25.50 rotor) at 40000xg for 40 min at 4°C. The soluble extract was incubated with 2 mL Streptactin XT beads (IBA Lifesciences) for 1 hour at 4°C. The beads were washed in HNG300, and proteins eluted with HNG300 supplemented with 10 mM biotin. Eluates were pooled and 30 mM imidazole was added. The binding of chaperone proteins was reduced by adding 5 mM Mg acetate and 5 mM ATP. Pooled proteins were incubated with 1 mL Ni-NTA beads (ThermoFisher Scientific) for 1 hour at 4°C. The beads were washed in HNG300 supplemented with 30 mM imidazole, and proteins eluted with HNG300 supplemented with 200 mM imidazole. Eluates were pooled, diluted to 100 mM NaCl (25 mM HEPES pH 8.0, 10% glycerol, 1 mM DTT) and loaded on to a pre-equilibrated 1ml HiTRAP Q HP column (GE Healthcare). Proteins were eluted with a linear gradient of 0.1 to 1 M NaCl and peak fractions identified by SDS-PAGE and Instant Blue (Gentaur) staining. Peak fractions were loaded into a Slide-A-Lyzer mini (ThermoFisher), dialyzed against 2 L storage buffer and frozen in liquid nitrogen. The SLX1-SLX4$^{CCD}$ concentration was determined to be 609 nM (assuming a 1:1 stoichiometry).

### DNA substrates
Oligonucleotides (Sigma Aldrich) were purified by 12% denaturing PAGE, ethanol precipitated and resuspended in TE (10 mM Tris-HCl pH 8.0, 1 mM EDTA). Radiolabeling and annealing was conducted as described (Rass and West, 2006). DNAs were prepared by annealing the following oligonucleotides: dsDNA (1 and 2), G/T mismatch (1 and 3), (CA)$_4$ loop (1 and 4), (CAG)$_{13}$ loop (1 and 5), and Holliday junction X0 (X0-1, X0-2, X0-3 and X0-4) (Chan and West, 2015). Oligonucleotide sequences are listed in Table S2:

For bio-layer interferometry (BLI) experiments, oligonucleotides (1–5 and X-01–04) were purified on a 12% denaturing PAGE, extracted in TE with 100 mM NaCl (10 mM Tris-HCl pH 7.5, 1 mM EDTA) and ethanol precipitated. Oligonucleotides 1 and X-01 were purchased 5′- biotinylated (Sigma Aldrich) prior to purification.

To generate biotinylated DNA substrates, 20 μM (for oligonucleotides 5′ biotin-1, 2, 3, 4 and 5) and 25 μM (for oligonucleotides 5′ biotin-X-01, X-02, X-03 and X-04) of gel purified oligonucleotides were annealed in a 1:1 molar ratio, followed by purification on a 15% native PAGE and ethanol precipitation.

### Recombination intermediates
Recombination intermediates containing a single HJ (α-structures) were generated by RecA-mediated strand exchange using gapped circular pDEA-7Z and 3′-$^{32}$P-end labeled linearized pDEA2 plasmid DNA, as described (Shah Punatar and West, 2018). Purified α-structures were stored at 4°C in 20 mM Tris-HCl, pH 8.0, 5 mM MgCl$_2$, 1 mM DTT and 100 μg/ml BSA.

### DNA binding assays
Electromobility shift assays (EMSAs) were conducted by incubating purified proteins with radiolabeled DNAs (3 nM) in buffer (50 mM Tris-HCl pH 8.0, 10 mM NaCl, 2 mM MgCl$_2$, 1% glycerol, 0.1 mg/ml BSA, 1 mM DTT) supplemented with competitor DNA (0.5 ng/μl poly[dIdC]) and 1 mM ADP, 1 mM ATP or 5 mM EDTA as indicated, for 10 min at room temperature. For reactions involving SLX4 or SLX1-SLX4$^{CCD}$, MutSβ or MutSα were pre-incubated with DNA in reaction buffer for 10 min at room temperature, SLX4/ SLX1-SLX4$^{CCD}$ was then added, and the reactions were incubated for a further 10 min at room temperature. Reactions were then transferred to ice and subjected to PAGE through a 5% bis-acrylamide gel in 0.5x TBE buffer at 150V for 1 hour at 4°C. Gels were dried onto Whatmann DE81 backed by 3 mm chromatography paper (Sigma-Aldrich) and the products were visualized by autoradiography. DNA binding was quantified by phosphoimaging and are described as a percentage of total DNA (see "Quantification and statistical analysis").

### Bio-layer interferometry

The interactions between MutSβ and DNA substrates ((CA)$_4$ and (CAG)$_{13}$ loops, HJ X0, G/T mismatch and dsDNA) were monitored by bio-layer interferometry (BLI) in 25 mM HEPES pH 8.0, 100 mM NaCl, 2 mM MgCl$_2$, 1 mM ADP/ATP, 0.1 mg/ml BSA, 1 mM DTT and 0.05% Tween-20 using an Octet RED96 system (FortéBio). A layer of biotinylated DNA (2 μg/ml) was immobilized on equilibrated Streptavidin biosensors (Dip and Read$^{TM}$) and incubated with a concentration range of MutSβ (500, 250, 125, 62.5, 31.25, 15.6, 7.8, 3.9 nM). The association of MutSβ to different DNA substrates was recorded until equilibrium had been reached, followed by a short dissociation. Data Acquisition 9.0 software (FortéBio) was used to record binding events. All measurements were carried out at 25°C, 1000 rpm on 96-well black flat-bottom plates with a volume of 200-250 μL per well. Biological duplicates were performed using freshly prepared DNA and protein solutions in independent experiments. Equilibrium dissociation constants (K$_d$) were obtained by plotting association amplitudes at equilibrium versus protein concentration. The data were fitted assuming a 1:1 interaction model, using non-linear least-squares regression by an in-house software.

### DNA cleavage assays

For reactions involving nucleases only, radiolabeled DNAs (10 nM) were pre-incubated in reaction buffer for 10 min at 37°C. The relevant nuclease(s) were then added, samples were taken at the indicated time points and stopped by addition of 2 mg/ml proteinase K (Promega) and 0.5% SDS for 30 min at 37°C. For experiments involving MutSβ or MutSα, radiolabeled DNAs (10 nM) were pre-incubated in reaction buffer supplemented with the indicated nucleotide (1 mM) for 10 min at 37°C. MutSβ or MutSα was added and DNA binding allowed to take place for 10 min. The relevant nuclease was then added, and samples were taken at the indicated time points. Cleavage reactions were stopped by addition of 2 mg/ml proteinase K (Promega) and 0.5% SDS for 30 min at 37°C. For analysis by neutral PAGE, 6x purple DNA loading dye (NEB) was added to the reactions and they were subjected to electrophoresis through a 10% bis-acrylamide (37.5:1) TBE gel at 150V for 1 hour at room temperature. Following electrophoresis, gels were dried onto Whatman DE81 backed by 3mm chromatography paper (Sigma-Aldrich) and the products were analyzed by autoradiography. DNA cleavage was quantified by phosphoimaging and is described as a percentage of total DNA (see "Quantification and statistical analysis").

### Recombination intermediate cleavage assays

SMX and MutSβ proteins were diluted in 50 mM Tris-HCl, pH 8.0, 100 mM NaCl, 10% glycerol, 1 mM dithiothreitol and 100 μg/ml BSA prior to use. SMX complex (0.1 nM) was preincubated with MutSβ (1-5 nM), or enzyme dilution buffer, for 5 min at 4°C followed by 10 min at 37°C, in cleavage buffer supplemented with 1 mM MgCl$_2$ and 1 mM ATPγS. 3′-$^{32}$P-labeled α-structures were then added (3 μM) and incubation continued for a further 15 min at 37°C. Reactions (10 μl) were carried out in cleavage buffer (50 mM Tris-HCl, pH 8.0, 1 mM DTT and 100 μg/ml BSA). Addition of the DNA contributed an additional 1.5 mM MgCl$_2$ to provide optimal cleavage conditions for SMX. Control reactions contained *E. coli* RuvC (10 nM) in cleavage buffer supplemented with 10 mM MgCl$_2$, RuvC was diluted in 20 mM Tris-HCl, pH 8.0, 50 mM NaCl, 20% glycerol, 1 mM DTT and 100 μg/ml BSA, prior to use. All reactions were stopped by the addition of 2 μL 6 x NEB purple loading dye, and DNA products were separated by 1.2% agarose gel electrophoresis in the presence of 0.5 μg/ml ethidium bromide. Gels were dried onto DE81 paper and $^{32}$P-labeled DNA detected by autoradiography and phosphorimager analysis.

### Immunofluorescence

Cells grown on coverslips were fixed with PTEMF buffer (20 mM PIPES pH 6.8, 0.2% Triton X-100, 1 mM MgCl$_2$ 10 mM EGTA and 4% paraformaldehyde) for 10 min. Cells were permeabilized with PBS containing 0.2% Triton X-100 for 5 min, then blocked in PBS supplemented with 3% BSA for 30 min. Coverslips were incubated with primary antibodies diluted in PBS and BSA for 1 hour, washed 3 × 5 min with PBS, and then incubated with secondary antibodies diluted in PBS and BSA for 1 hour. Coverslips were washed 3 × 5 min with PBS and mounted using Prolong Diamond antifade reagent (ThermoFisher). See "Antibodies" for details of the antibodies used.

### Microscopy

Images were acquired with an AXIO Imager M2 microscope (Zeiss) using a plan-APOCHROMAT 63x 1.4 oil objective (Zeiss) and Hamamatsu photonics camera. Imaging was conducted using Volocity software (PerkinElmer) and images processed in Adobe Photoshop.

## QUANTIFICATION AND STATISTICAL ANALYSIS

All gel quantifications were obtained by overnight phosphoimaging with a BAS-IP TR 2025 E Tritium Storage Phosphoscreen (Sigma), followed by imaging using a Typhoon FLA 9500 scanner (GE Healthcare). Cleavage products were quantified as a percentage of total radiolabeled DNA using ImageQuant TL v8.1. Unless indicated otherwise, data is presented as the mean of three independent experiments ± SD. Statistical analysis was performed using the student two-tailed t test. A *p-value* of less than 0.05 was considered statistically significant.